HHS Public Access

Author manuscript

Histochem Cell Biol. Author manuscript; available in PMC 2022 June 01.

Published in final edited form as:

Histochem Cell Biol. 2021 June ; 155(6): 699–718. doi:10.1007/s00418-021-01978-x.

Organic Dust Exposure Induces Stress Response and Mitochondrial Dysfunction in Monocytic Cells

Sanjana Mahadev Bhat[1], **Denusha Shrestha**[1], **Nyzil Massey**[1], **Locke A. Karriker**[2], **Anumantha G. Kanthasamy**[1], **Chandrashekhar Charavaryamath**[1,*]

[1]Department of Biomedical Sciences, 2008 Vet Med Building, Iowa State University, Ames, IA, USA.

[2]Department of Veterinary Diagnostic and Production Animal Medicine, 2203 Lloyd Veterinary Medical Center, Iowa State university, Ames, IA, USA

Abstract

Exposure to airborne organic dust (OD), rich in microbial pathogen-associated molecular patterns (PAMPs), is shown to induce lung inflammation. A common manifestation in lung inflammation is altered mitochondrial structure and bioenergetics that regulate mitochondrial ROS (mROS) and feed a vicious cycle of mitochondrial dysfunction. The role of mitochondrial dysfunction in other airway diseases is well known. However, whether OD exposure induces mitochondrial dysfunction remains elusive. Therefore, we tested a hypothesis that organic dust extract (ODE) exposure induces mitochondrial stress using a human monocytic cell line (THP1). We examined whether co-exposure to ethyl pyruvate (EP) or mitoapocynin (MA) could rescue ODE exposure induced mitochondrial changes. Transmission electron micrographs showed significant differences in cellular and organelle morphology upon ODE exposure. ODE exposure with and without EP co-treatment increased the mtDNA leakage into the cytosol. Next, ODE exposure increased PINK1, Parkin, cytoplasmic cytochrome c levels, and reduced mitochondrial mass and cell viability, indicating mitophagy. MA treatment was partially protective by decreasing Parkin expression, mtDNA and cytochrome c release and increasing cell viability.

Keywords

Organic dust; mitoapocynin; ethyl pyruvate; mitochondrial dysfunction; mitochondrial DNA

[*]To whom correspondence should be addressed: Chandrashekhar Charavaryamath, BVSc, MVSc, PhD., Assistant Professor, Department of Biomedical Sciences, Iowa State University, Ames, IA 50011. Telephone: (515) 294-7710; Fax: (515) 294-2315; chandru@iastate.edu.

Author contributions

S.M. Bhat participated in the design of experiments, performed the experiments, analyzed the data, and wrote the manuscript. D. Shrestha performed the calcium influx assay. N. Massey performed organic dust extraction. L. Karriker collected the organic dust samples and edited the manuscript. A.G. Kanthasamy provided mitoapocynin and edited the manuscript. C. Charavaryamath conceptualized the study, participated in the design of the experiments, performed dust extraction, participated in the interpretation of data and edited the manuscript. All authors have read and approved the final manuscript.

Potential Conflicts of Interest

AGK has an equity interest in PK Biosciences Corporation located in Ames, IA.

The terms of this arrangement have been reviewed and approved by Iowa State University per its conflict of interest policies. All other authors have declared no potential conflicts of interest.

Availability of data and material

The data generated during the current study are available from the corresponding author upon reasonable request.

Introduction

Industrialized agriculture production systems form the backbone of farm economy in the USA with a large number of workforce and a significant contribution to the nation's GDP (Charavaryamath and Singh 2006; Sethi et al. 2017; Nordgren and Charavaryamath 2018). Despite the production efficiency and cheaper price of food, these industries have occupational hazards in the form of exposure to many on-site contaminants. Among the contaminants, airborne organic dust (OD) and gases (mainly hydrogen sulfide, methane and ammonia), viable bacteria, fungal spores and other microbial products are known to be present (Vested et al. 2019). Bacterial lipopolysaccharide (LPS) and peptidoglycan (PGN) are the major microbial pathogen associated molecular patterns (PAMPs) present in OD (May et al. 2012). Agriculture production workers who are exposed to OD report several respiratory symptoms and annual decline in the lung function (Wunschel and Poole 2016; Sethi et al. 2017; Nordgren and Charavaryamath 2018).

Persistent exposure to OD has been linked to the development of chronic inflammatory conditions, such as chronic obstructive pulmonary disease (COPD) and asthma, including lung tissue damage and decline in lung function (Charavaryamath and Singh 2006; Wunschel and Poole 2016). Despite several research groups using both *in vitro* and *in vivo* models of OD exposure, precise cellular and molecular mechanisms responsible for the development of these chronic lung diseases remain largely unknown. In order to design effective therapeutic strategies against OD-induced airway diseases, an understanding of the underlying mechanisms of airway inflammation is essential. Studies have shown that OD-mediated lung inflammation is typically characterized by airway hyperresponsiveness (AHR), tissue remodeling, and increased influx of inflammatory cells, particularly neutrophils and macrophages (Charavaryamath et al. 2005; Sahlander et al. 2012; Sethi et al. 2017). In previous studies, we have shown that exposure of human bronchial epithelial cells to OD results in the production of reactive oxygen species (ROS), reactive nitrogen species (RNS), and a myriad of pro-inflammatory cytokines such as interleukins IL-1β, IL-6, and IL-8 (Nath Neerukonda et al. 2018; Bhat et al. 2019). Production of pro-inflammatory mediators, development of abnormal mitochondrial signatures and mitochondrial dysfunction have been shown to contribute to the pathological mechanisms underlying airway diseases (Cloonan and Choi 2016). Mitochondria are emerging as a central focal point in many inflammatory airway diseases (Su et al. 2016; Prakash et al. 2017). Collectively, these findings suggest that instead of targeting multiple pattern recognition receptors (PRRs), focusing on mitochondrial dysfunction appears to be a more promising single common target to curtail the inflammation (Charavaryamath et al. 2008; Poole et al. 2010; Poole et al. 2011).

The role of mitochondria in OXPHOS, stress responses and programmed cell death pathways have been well studied over the past decade, the role of mitochondria in the sustained lung inflammation is of great interest (Prakash et al. 2017). Studies have demonstrated the elevation of critical enzymes involved in the production of ROS and RNS due to mitochondrial impairment in various inflammatory conditions (Zhang et al. 2010; Cloonan and Choi 2012; Eisner et al. 2018). Dysfunctional mitochondria result in impaired

cellular respiration, compromised cellular immune response and cell death. (Cloonan and Choi 2012; Eisner et al. 2018).

The adverse effects of inflammation on mitochondria can be abrogated by several mechanisms. These include the induction of antioxidant defenses, maintenance of mitochondrial integrity through the selective removal of dysfunctional mitochondria (mitophagy), and the generation of new organelles to replace damaged or dysfunctional mitochondria through mitochondrial biogenesis (Eisner et al. 2018). However, the integration of these compensatory responses, and the interaction between mitochondria and host cells following OD exposure, are not well understood. Previously, we have shown that, damage-associated molecular patterns (DAMPs) such as high mobility group box 1 (HMGB1) have a role to play in OD-induced airway epithelial inflammation (Bhat et al. 2019). Further, using a microglial model of OD-exposure, we confirmed the role of HMGB1 in inducing neuroinflammation where our data indicated involvement of mitochondria in OD-induced reactive species generation and neuroinflammation (Massey et al. 2019). We also showed that using ethyl pyruvate (EP, blocks translocation of HMGB1) or anti-HMGB1 neutralizing antibodies, OD-induced inflammation could be abrogated (Bhat et al. 2019).

The protective effects of EP have been attributed to its anti-inflammatory, antioxidative and antiapoptotic actions as well as its ability to prevent phosphorylation and release of HMGB1 (Shin et al. 2014). We also demonstrated that EP downregulates OD-induced reactive oxygen species (ROS) generation and augments IL-10 production to promote anti-inflammatory effects. (Bhat et al. 2019). Similar results have been shown in LPS injected and ischemic animal models as well (Venkataraman et al. 2002; Yu et al. 2005). Other anti-inflammatory properties of EP have been attributed to the inhibition of ROS-dependent signal transducer and activator of transcription (STAT) signaling (Kim et al. 2008; Shin et al. 2014).

Another potent mitochondrial specific antioxidant we have used previously is mitoapocynin (MA) (Massey et al. 2019). Apocynin, a plant derived antioxidant, has been used as an efficient inhibitor of cytoplasmic NADPH-oxidase complex (NOX2) in many experimental models involving phagocytic and nonphagocytic cells (Stefanska and Pawliczak 2008). Mitoapocynin (MA) is a triphenylphosphonium (TPP) conjugated apocynin designed to enhance cellular uptake of the compound and target the mitochondria. In contrast to other popular antioxidant therapies, MA has been shown to suppress production of iNOS and various pro-inflammatory cytokines in various neuroinflammatory disease models. In addition, MA was shown to inhibit cytoplasmic NOX2 activity and reduce oxidative stress (Ghosh et al. 2016; Langley et al. 2017).

In this study we used an immortalized human monocytic cell line (THP1) and tested a hypothesis that OD-exposure induces mitochondrial stress. We further examined whether induction of antioxidant defenses with either EP or MA treatment changes mitochondrial biogenesis in THP1 cells following exposure to ODE. Here we demonstrate that mitochondrial targeting apocynin (MA) that inhibits cytoplasmic NOX2 or pharmacological inhibition of HMGB1 translocation (EP), are vital to cellular recovery following exposure to OD.

Materials and Methods

Chemicals and reagents

We purchased RPMI 1640, L-glutamine, penicillin-streptomycin, MitoTracker green dye, and MitoSOX Red dye from Invitrogen (ThermoFisher Scientific) and fetal bovine serum (FBS) was purchased from Atlanta Biologicals (Flowery Branch, GA, catalog # S11150H and lot # A17002). Antibodies for mitofusins (MFN1/2), DRP1, PINK1, Parkin, OPA1, BNIP3, Cytochrome C, COX4i2, Bcl-2, Bcl-XL, mtTFA, Caspase 1 and Caspase 3 was purchased from Santa Cruz Biotechnology. The anti-HMGB1 antibody, β-Actin antibody and Rhod-2AM dye were obtained from Abcam. The details of the antibodies used are listed in Table 1 and Table 2. MitoApocynin-C_2 (MA) was procured from Dr. Balaraman Kalyanaraman (Medical College of Wisconsin, Milwaukee, WI), stock solution (10 mM in DMSO) prepared by shaking vigorously and stored at −20°C. MA was used (10 μM) as one of the co-treatments. Ethyl pyruvate (EP, Santa Cruz Biotechnology, Dallas, TX), was reconstituted in Ringer's solution (Sigma-Aldrich) and used at a final concentration of 2.5 μM in the cell culture medium (Ghosh et al. 2016; Langley et al. 2017).

Organic dust extract preparation

Aqueous organic dust extract (ODE) was prepared as previously described (Romberger et al. 2002; Bhat et al. 2019). Settled surface dust samples from swine production units were collected, and 1 g of the dust was placed into sterile Hank's Balanced Salt Solution (10 mL; Gibco). The solution was incubated for one hour at room temperature, centrifuged for 20 min at 1365 x g, and the final supernatant was filter-sterilized (0.22 μm), a process that removes coarse particles. Stock (100%) aliquots of ODE samples were kept frozen at −20°C until used in experiments. The filter-sterilized organic dust extract (ODE) samples were considered 100% and diluted to 1-5% (v/v) before using in the experiments. We routinely measure LPS concentration in our ODE samples using Pyrochrome® chromogenic endotoxin assay kit (Associates of Cape Cod, Inc., East Falmouth, MA). As per previously published study, the LPS concentrations found in our ODE samples were in the range of 0.8067±0.0008 to 1.433±0.02 EU/mL (Bhat et al. 2019).

Cell culture and treatments

Immortalized human monocytic cells (THP1, ATCC TIB-202™) were used in this study. The cells were characterized prior to use in experiments by confirming expression of CD14 using flow cytometry (data not shown). This cell line has previously been used by our group to study innate inflammatory responses to ODE (Nath Neerukonda et al. 2018). THP1 cells were cultured in RPMI 1640 at 37°C in a humidified chamber with 5% CO_2. The RPMI 1640 medium was supplemented with 10% (v/v) heat-inactivated FBS, 2 mM L-glutamine, 10 mM HEPES, 1.5 g/L sodium bicarbonate, 1 mM sodium pyruvate, 100 IU/ml penicillin, and 100 μg/mL streptomycin and 1 μg/mL of Amphotericin B. Cells were sub cultured once a week, the morphology was observed and approximately 4 to 5-day old cultures in suspension were used for all the experiments. Treatments were added to the cells in 1% FBS-containing medium for 24 hours and the treatment details (groups) are outlined in Figure 1.

The stock and working concentrations of the treatments are outlined in Table 3. Cells were treated with either medium (control) or ODE (1% v/v) followed by a co-treatment with either EP (2.5 μM)(Bhat, et al., 2019) or MA (10 μM)(Massey, et al., 2019) for 24 hours, with corresponding time matched controls. Following treatments, samples were processed at 24 hours for various assays. The concentration of DMSO used in our experiments was not toxic to cells (data now shown) and MA is well tolerated in higher doses (Anantharam et al. 2007; Cristóvão et al. 2009).

Cell viability and MTT assay

Live/dead cell numbers were enumerated by 4% trypan blue dye (EMD Millipore) exclusion and the percentage viability was calculated. Population of cells with more than 95% viability were used for the experiments. The MTT assay has been widely used in the estimation of LC_{50} and cell viability by measuring the formazan produced when mitochondrial dehydrogenase enzymes cleave the tetrazolium ring (Latchoumycandane et al. 2005). In this study, we used the MTT assay to determine the LC_{50} of ODE in THP1 cells. Cells were seeded (20,000 cells/well) in a 96-well culture plate and treated with ODE, EP, and MA for 24 hours in 1% FBS-containing RPMI medium. After treatment, the cells were washed twice with PBS and incubated with 0.5 mg/mL of MTT in 1% FBS-containing RPMI medium for 3 hours at 37°C. The supernatant was removed, and MTT crystals were solubilized in 100 μl of DMSO. Absorbance was measured with the SpectraMax M2 Gemini Microplate Reader (Molecular Devices, San Jose, CA) at 570 nm with the reference wavelength at 630 nm.

Transmission Electron Microscopy (TEM)

Following the treatments (Table 3), cells were washed twice with RPMI and fixed with 3% glutaraldehyde (w/v) and 1% paraformaldehyde (w/v) in 0.1 M cacodylate buffer, pH 7.4 for 48 hours at 4°C. Cells were pelleted and resuspended into 1% agarose. Small (1 mm) cubes containing cells were cut from the agarose and processed. Samples were rinsed three times in 0.1 M cacodylate buffer and then post-fixed in 1% osmium tetroxide in 0.1 M cacodylate buffer for 1 hour (room temperature). The samples were rinsed in deionized distilled water and *enbloc* stained with 2% aqueous uranyl acetate for 30 min., dehydrated in a graded ethanol series, cleared with ultra-pure acetone, infiltrated and embedded using EmBed (EPON) formula epoxy resin (Electron Microscopy Sciences, Ft. Washington, PA). Resin blocks were polymerized for 48 hours at 65°C. Thick and ultrathin sections were prepared using a Leica UC6 ultramicrotome (North Central Instruments, Minneapolis, MN). Ultrathin sections were collected onto copper grids and images were captured using a JEOL 2100 scanning and transmission electron microscope (Japan Electron Optic Laboratories, Peabody, MA) with a Gatan OneView 4K camera (Gatan inc., Pleasanton, CA).

Morphological analysis

Mitochondrial shape descriptors and size measurements were obtained using ImageJ (National Institutes of Health) by manually tracing only clearly discernible outlines of mitochondria on TEM micrographs (Picard et al. 2013). Surface area (or mitochondrial size, in μm^2); perimeter (in μm), circularity [4*(surface area/perimeter^2)]; and Feret's diameter, which represents the longest distance (μm) between any two points within a given

mitochondrion, were measured. Computed values were imported into Microsoft Excel and analyzed.

Subcellular fractionation

Whole cell and subcellular (cytosol and mitochondria) protein lysate extractions were performed at 4°C using cold reagents. Subcellular fractionation of cell pellets for isolation of mitochondria was done using the Mitochondria Isolation Kit for Cultured Cells (ThermoFisher Scientific) according to the manufacturer's instructions. The whole cells, cytosolic fraction and isolated mitochondria were lysed with RIPA buffer [with protease and phosphatase inhibitors] for 30 min at 4°C and periodic sonication on ice, followed by centrifugation to collect lysate. Protein concentration of the fractions were determined by Bradford assay (Bio-Rad) and were stored at −80°C until use.

Mt DNA isolation and long-range PCR

To determine mitochondrial DNA (mtDNA) leakage into cellular cytosol, mtDNA was isolated from mitochondria-free cytosolic fraction of the cells using the Genomic DNA Purification kit (ThermoFisher Scientific) as per the manufacturer's instructions. The purity and concentration of the isolated DNA was measured using NanoVue Plus Spectrophotometer (GE Healthcare). Due to low concentrations, the mtDNA was first amplified using long range PCR and the primers used were: mtDNA plasmid, sense: 5′-TGAGGCCAAATATCATTCTGAGGGGC-3' and antisense: 5′-TTTCATCATGCGGAGATGTTGGATGG-3' (Liu et al. 2015). PCR reactions were performed at 94°C for 1 min followed by 30 cycles at 98°C for 10 s, 60°C for 40 s, 68°C for 16 min and a final elongation for 10 min (Liu et al. 2015). Presence of mtDNA was confirmed by separating the PCR product by electrophoresis on a 0.8% agarose gel stained with ethidium bromide. The concentration of amplified mtDNA obtained was adjusted to ensure equal amounts of template mtDNA in each sample used for qPCR reaction.

Quantitative Real-Time PCR

Fold change in mtDNA quantity was measured by qPCR with primers specific to mitochondrial NADH dehydrogenase 1 (*mtND1*). 10 μL reaction mixtures with 500 ng of template DNA and 1 μM of forward and reverse primers in SYBR Green Mastermix (Thermo Fisher Scientific) was prepared. The primers for genes of interest were synthesized at Iowa State University's DNA Facility. The primers used were: *mtND1* gene, sense: 5'-GGCTATATACAACTACGCAAAGGC-3' and antisense: 5'-GGTAGATGTGGCGGGTTTTAGG-3'; *16s* (housekeeping gene), sense: 5'-CCGCAAGGGAAAGATGAAAGAC-3' and anti-sense: 5'-TCGTTTGGTTTCGGGGTTTC-3'. No-template and no-primer controls and dissociation curves were run for all reactions to exclude cross-contamination. The qRT-PCR reactions were run in a QuantiStudio 3 system (ThermoFisher) and the data was analyzed using 2^{-DDCT} method (Livak and Schmittgen 2001).

Western blot analysis

Lysates (whole cell, cytosol and MT) containing equal amounts of protein (20 μg/sample), along with a molecular weight marker (Bio-Rad), were run on 10–15% sodium dodecyl sulfate/polyacrylamide gel electrophoresis (SDS-PAGE) as previously described (Bhat et al. 2019). Proteins were transferred to a nitrocellulose membrane and nonspecific binding sites were blocked with Licor Odyssey blocking buffer. The membranes were then incubated with different primary antibodies, the details of which are listed in Table 1. Next, membranes were incubated with one of the following secondary antibodies: Alexa Fluor 680 goat anti-mouse, Alexa Fluor 680 donkey anti-rabbit (1:10,000; Invitrogen) or IRDye® 800CW donkey anti-rabbit (1:10,000; LI-COR) (Table 2). To confirm equal protein loading, blots were probed with a β-actin antibody (AbCam; 1:10,000 dilution). Western blot images were captured using Odyssey® CLx IR imaging system (LI-COR Biotechnology) and analysis was performed using ImageJ (National Institutes of Health). The results were represented as a percentage expression relative to control.

Mitochondrial activity and MitoSOX assay

Cells were seeded (50,000 cells/well) in a 96-well culture plate and treated for 24 hours. After treatment, the media was removed and 100 μL of 200 nM MitoTracker green and 5 μM MitoSOX red dye diluted in 1% FBS-containing RPMI medium was added into each well and incubated at 37°C for 15 min. Next, the cells were washed with 1% FBS-containing RPMI medium and fluorescence intensity was measured by spectrophotometer reading taken at excitation/emission wavelengths of 485/520 nm and 510/580, respectively (SpectraMax M2 Gemini Microplate Reader, Molecular Devices, San Jose, CA). The results were represented as percentage mean fluorescence intensity (% MFI) relative to control.

Mitochondrial calcium influx measurement by rhod-2AM staining

Mitochondrial calcium influx ($[Ca^{2+}]_{mito}$) in THP1 cells was measured using the rhod-2AM dye. The protein concentration of the isolated mitochondrial fraction was measured by Bradford assay in order to maintain consistency in the number of mitochondria loaded into the wells of a 96-well plate. Equal amounts of protein (100 μg) were loaded into each well and10 μM Rhod-2AM (Abcam) dye diluted in 1% FBS-containing RPMI medium was added and incubated at 37°C for 30 minutes. The cells were washed with 1% FBS-containing RPMI medium and fluorescence was read at excitation/emission wavelengths of 552 nm/581 nm using a spectrophotometer reader (SpectraMax M2 Gemini Microplate Reader, Molecular Devices, San Jose, CA) and results represented as percentage calcium influx.

Griess assay

Griess assay was performed as described previously (Gordon et al. 2011). Nitric oxide secretion was measured (representing reactive nitrogen species (RNS)) in cell culture media using Griess reagent (Sigma-Aldrich) along with sodium nitrite standard curve, prepared using a stock solution of 200 μM. The assay was performed in a 96 well-plate and absorbance was measured at 550 nm (SpectraMax M2 Gemini Microplate Reader,

Molecular Devices, San Jose, CA). The results were represented as μM concentration of nitrite secreted.

Cytokine analysis

Levels of IL-1β, IL-6, TNF-α and IL-10 in the cell culture supernatant were measured using commercially available ELISA kits (ThermoFisher Scientific, USA) as per the manufacturer's instructions. 96-well high binding plates (Nunc MaxiSorp, ThermoFisher Scientifc) were coated with the capture antibody (100 μL/well) and incubated at 4 °C overnight. All the wells were blocked with the blocking buffer (200 μL/well) for an hour at room temperature followed by washing with PBS-T and then, incubated with recombinant standards and samples (cell culture supernatants) for 2 h at room temperature. Next, plates were washed with PBST and incubated with the specific detection antibody (100 μL/well) for 1 h at room temperature. Following a wash, the plates were then incubated with 3,3′,5,5′-tetramethylbenzidine (TMB) solution (100 μL/well) for 15 min and the reaction (color development) was stopped by adding 50 μL/well of the stop solution (2 N H_2SO_4). The absorbance was read at 450 nm (SpectraMax M2 Gemini Microplate Reader, Molecular Devices, San Jose, CA) and the results (concentration of cytokine secreted) were represented as pg/mL.

Statistical analysis

Data analysis and graphical representation was performed using GraphPad Prism 8.0 software (GraphPad Prism 8.0, La Jolla, CA, USA). Data was analyzed with one-way ANOVA with Tukey's multiple comparison test and a p-value of < 0.05 was considered to be statistically significant.

Results

Endotoxin levels in ODE samples

Endotoxin content of diluted ODE (1:10) samples was measured. From three samples collected we found that endotoxin values ranged from 0.99 ± 0.0005 to 1.433 ± 0.02 EU/mL.

Exposure to ODE impacts the cellular and mitochondrial morphology

TEM images showed that THP1 cells treated with media alone (controls) displayed normal morphology with healthy mitochondria (Fig. 2a-d and 3a-d). Following ODE treatment, cytoplasmic vacuolization and pseudopod formation was observed suggesting differentiation of cells (Fig. 2b) (Krysko et al. 2006). In addition, the mitochondria appeared larger in size and some of the mitochondria were elongated with reduced cristae numbers and/or appearance of deformed cristae (Fig. 3b). On addition of EP, similar to ODE exposure, the mitochondria were swollen and showed disorganized cristae, along with the presence of calcium sequestration bodies in the mitochondrial matrix (Fig. 3c). In contrast, exposure to MA seemed to restored the impact of ODE. Cells exposed to both ODE and MA showed almost no cytoplasmic vacuolization, and mitochondria showed decreased signs of damage to cristae, albeit conformed to an elongated morphology (Fig. 2d and 3d). These results suggest that MA has a partial protective effect on ODE exposed macrophages.

In order to quantify ultra-structural changes observed in the TEM images, mitochondria were individually traced from the micrographs. Compared to controls, exposure to ODE significantly reduced the mitochondrial surface area (Fig. 3e). A similar decrease was seen in the presence of MA as well, whereas EP significantly increased the surface area (mitochondrial size) comparable to that of control group (Fig. 3e). Compared to controls, treatment with ODE and with either EP or MA decreased the mitochondrial circularity. Among these, cells co-treated with ODE with MA showed maximum decrease in mitochondrial circularity (Fig. 3f). Other morphological parameters such as perimeter, and Feret's diameter did not differ between any of the treatment groups (Fig. 3g and 3h).

Targeted antioxidant therapy promotes mitochondrial fission

The mitochondrial membrane is continuously remodeled through cycles of fission and fusion events. In order to accurately interpret the impact of ODE exposure on mitochondrial morphology, expression of markers responsible for the dynamic events was measured. On ODE exposure, the expression of mitofusin 2 (MFN2) was significantly increased compared to control (Fig. 4a and 4c). In contrast, mitofusin 1 (MFN1) and optic atrophy 1 (OPA1) protein levels were not different among any of the treatment groups compared to control (Fig. 4a, 4b and 4d). Increased expression of dynamin-related protein 1 (DRP1) was observed in cells treated with both ODE and ODE with MA (Fig. 4e and 4f). Furthermore, to analyze changes in mitochondrial number, change in mitochondrial mass was measured using mitotracker green dye. There was a significant increase in the mitochondrial mass on exposure to ODE and ODE with EP, while on exposure to MA mitochondrial mass decreased comparable to controls in size (Fig. 4g).

ODE exposure induces selective targeting of mitochondria for autophagy (mitophagy)

We investigated whether ODE exposure induces mitophagy-mediated clearance of mitochondria. The expression of the two important mediators of mitophagy, PTEN-induced kinase 1 (PINK1) and the E3 ubiquitin protein ligase Parkin, were investigated. Compared to controls, ODE exposure increased the expression of Parkin but not PINK1 (Fig. 5a and 5c). Further, co-treatment with EP and MA reversed the ODE induced increase in Parkin (Fig. 5a and 5b). The expression of BNIP3, a mitochondrial Bcl-2 Homology 3 (BH3)-only protein, was also observed. BNIP3 levels remained unchanged on exposure to ODE and ODE with EP (Fig. 5a and 5d). While co-treatment with MA significantly decreased BNIP3 expression (Fig. 5d).

ODE exposure impacts mitochondrial membrane permeability

Mitochondrial oxidative phosphorylation (OXPHOS) pathway is critical in determining and maintaining the immunomodulatory phenotype of activated macrophages (Kelly and O'Neill 2015). Considering this mitochondrial OXPHOS pathway was investigated. ODE exposure increased the levels of cytosolic cytochrome c, compared to that in the mitochondrial fraction indicating the release of cytochrome c from the mitochondria (Fig. 6a-6c). On the other hand, MA treatment significantly decreased ODE-induced release of cytochrome c into the cytosol (Fig. 6a-6c). Following ODE exposure there was a significant decrease in the expression of lung-specific isoform of cytochrome c oxidase (COX4i2) in the mitochondrial fraction and there was no change in COX4i2 levels following treatments with either EP or

MA (Fig. 6d and 6f). For all treatment groups expression of SOD2 significantly increased compared to controls, while treatment with EP or MA decreased the levels when compared to cells exposed to ODE alone (Fig. 6e and 6g). Presence of SOD2 is known to impart tolerance during high oxidative stress and reduce superoxide accumulation withing the mitochondria (Fukui and Zhu 2010; Ishihara et al. 2015). To identify whether this is true, mitochondrial superoxide levels were measured using MitoSOX dye. Exposure to ODE significantly decreased the mitochondrial superoxide, while treatment with MA increased the levels similar to control (Fig. 6h). Using the Griess assay, we measured the reactive nitrite species (RNS) released into the extracellular environment. ODE exposure increased the levels of RNS in the cell culture media at 24 hours, while treatment with EP and MA significantly attenuated the RNS secretion (Fig. 6i).

ODE induces the secretion of mitochondrial DAMPs

Mitochondrial secondary messengers can act as mitochondrial damage–associated molecular patterns (mtDAMPs) when produced excessively or secreted into other cellular locations (Cloonan and Choi 2012). Compared to controls, ODE, ODE with EP or MA treatments showed increased levels of mitochondrial transcription factor A (mtTFA) expression in both the mitochondrial and cytosolic fractions (Fig. 7a-7c). On measuring the levels of mtDNA leaking into the cytosol, it was observed that exposure to ODE increased the cytosolic mtDNA levels, which was abrogated on treatment with EP or MA (Fig. 7d). In addition, there was an increase in calcium (Ca^{2+}) influx into the mitochondria in all treatment groups, with no significant change in the presence of either MA or EP co-treatment compared to ODE (Fig. 7e). The expression of mitochondrial HMGB1 was determined, as presence of HMGB1 in the mitochondrial matrix is known to be critical in the regulation of mitochondrial function (Tang et al. 2011). Compared to control, expression of mitochondrial HMGB1 was significantly decreased (Fig. 7f and 7g). In addition, we observed the presence of low molecular weight cleaved HMGB1 bands. However, upon quantification there were no significant differences between treatments (Data not shown). EP treatment significantly increased mitochondrial HMGB1 expression when compared to treatment with both ODE and ODE with MA (Fig. 7f and 7g).

Mitoapocynin does not intervene in ODE mediated caspase-1 upregulation

Published work shows that the release of mtDNA and mitochondrial reactive oxygen species (mROS) activates the NLRP3 inflammasome pathway (Gong et al. 2018). Upstream of NLRP3 activation, cleavage of pro-caspase 1 to caspase 1 is seen due to increased influx of calcium induced by leaky mitochondria (Murakami et al. 2012). Based on this, changes in the expression of pro-caspase 1 and caspase 1 were measured. Compared to control, exposure to ODE, ODE and EP or MA increased the expression of pro-caspase 1. ODE with EP treatment reduced pro-caspase 1 levels significantly when compared to ODE (Fig. 8a and 8b). Compared to controls, ODE and ODE with MA exposure significantly increased the expression of cleaved caspase 1 (p10). Treatment with EP significantly decreased cleavage compared to ODE, which is consistent with the expression of pro-caspase 1. Expression of pro-caspase 3 and its cleaved product was measured in order to determine if ODE is inducing a caspase 3 mediated apoptosis. Although ODE minimally decreased the expression of pro-caspase 3 compared to control, caspase 3 expression in ODE with EP or

MA treated cells remained unchanged (Fig. 8d and 8e). In addition, there was absence of caspase 3 cleavage product in any of the treatment groups (Fig. 8d).

Previously we have shown that ODE exposure of bronchial epithelial cells induces secretion of pro-inflammatory cytokines. We also showed that EP treatment significantly decreases the release of the pro-inflammatory cytokines, particularly IL-1β and increases the anti-inflammatory cytokine IL-10 production (Bhat et al. 2019). Consistent with previous studies, in this study levels of TNF-α, IL-1β and IL-6 were significantly increased in ODE exposed THP1 cells compared to controls (Supplementary fig. S1a-S1c). With EP or MA co-treatment, the levels were significantly reduced when compared to cells treated with ODE alone but were still higher compared to controls. Concentration of IL-10 was increased upon exposure to ODE with EP or MA, indicating initiation of an anti-inflammatory processes. This increase of IL-10 levels was not observed in THP1 cells exposed to ODE alone (Supplementary fig. S1d).

Mitoapocynin therapy does not inhibit ODE induced apoptosis

To identify the impact OD-induced mitochondrial dysfunction and rescue may have on cellular apoptosis, expression of Bcl-2 and Bcl-XL were measured. Decreased expression of Bcl-2 was observed among all treatment groups compared to controls with no significant impact on co-treatment with EP or MA (Fig. 9a and 9b). Compared to controls, ODE, ODE with EP or MA decreased the Bcl-XL expression. However, ODE with EP or ODE with MA treatment significantly increased Bcl-XL levels compared to ODE treated cells (Fig. 9d and 9e). This change in expression of Bcl-XL was corroborated by measuring cell viability by MTT colorimetric assay. The percentage cell viability observed correlated with the expression pattern of Bcl-XL, where loss of cell viability on ODE exposure was rescued by treatment with EP or MA (Fig. 9c).

Discussion

Chronic exposure to OD is a key contributor to the development of respiratory symptoms and airway obstruction in exposed workers (Cole et al. 2000; Nordgren and Charavaryamath 2018). Continuous exposure to OD has been shown to alter innate immune responses in the airways (Charavaryamath and Singh 2006; Wunschel and Poole 2016; Sethi et al. 2017). These responses include recruitment of inflammatory cells, release of pro-inflammatory cytokines and reactive species (ROS/RNS) (Sahlander et al. 2012; Sethi et al. 2017; Nath Neerukonda et al. 2018; Bhat et al. 2019). Previous studies have provided a direct link between such innate immune signaling events and mitochondrial dynamics suggesting a crucial role for mitochondria in the activation and control of airway disease progression (Cloonan and Choi 2012; Eisner et al. 2018). In this study, using THP1 cells as an *in vitro* model for alveolar macrophages, we demonstrate that OD exposure leads to significant changes in mitochondrial dynamics, integrity, and function. Next, using mitoapocynin (MA), a novel mitochondrial targeting NOX2 inhibitor, or ethyl pyruvate (EP), an inhibitor of translocation of HMGB1, we partially rescued ODE-induced mitochondrial changes and reduced the resultant inflammation.

Our TEM results demonstrate that, upon ODE exposure, there is an increased presence of cytoplasmic vacuoles and formation of pseudopods which is a characteristic feature of activated macrophages (Kim et al. 2008). Treatment with MA or EP did not prevent the ODE-induced morphological changes. To understand the impact of ODE-induced inflammation on mitochondrial biogenesis, we explored the factors involved in mitochondrial morphological changes. Mitochondria are highly dynamic organelles which continuously change their function, position, and structure to meet the metabolic demands of the cells during homeostatic conditions as well as at times of cellular stress (Wai and Langer 2016; Eisner et al. 2018). In this study, using TEM image analysis, we observed significant decrease in the mitochondrial surface area and circularity upon ODE exposure indicating that ODE-exposure could have an impact on mitochondrial dynamics and function. Similar exposure induced changes have been reported in previous studies as well (Westrate et al. 2014; Wai and Langer 2016; Eisner et al. 2018).

Exposure to toxic materials is known to alter mitochondrial morphology and biogenesis through fusion and fission (Fetterman et al. 2017). The delicate balance of these events helps in controlling mitochondrial structure and function (Wai and Langer 2016; Tilokani et al. 2018). Our results indicate that ODE exposure increased the expression of MFN2 but not MFN1 and OPA1. Thus ODE exposure mediated increase in MFN2 could be promoting mitochondrial fusion. Further, EP treatment significantly reduced ODE induced MFN2 expression indicating that blocking nucleocytoplasmic translocation of HMGB1 could possibly reduce mitochondrial fusion. Next, our results show an increase in DRP1 as well upon exposure to ODE, which is further increased on co-treatment with MA. DRP1 dependent mitochondrial fragmentation is characterized by decreased expression of OPA1, which is observed in ODE exposed cells treated with MA (Mishra and Chan 2014; Tilokani et al. 2018). An increase in the rate of mitochondrial fragmentation is possibly a cellular response to counteract the loss of mitochondrial function and recover ATP synthesis capacity. Inhibition of DRP1-mediated mitochondrial fission has been reported to cause cellular dysfunction and replication (Qi et al. 2015). This can be corroborated by the decrease in cell viability with ODE exposure. The decreased mitochondrial mass observed with exposure to ODE and MA could be a means by which the mitochondria targeted NOX2 inhibition (antioxidant therapy) is overcoming the increase in dysfunctional mitochondria via mitochondrial biogenesis and mitophagy, thus allowing cells to quickly replace metabolically dysfunctional mitochondria.

MFN2 is known to mediate the recruitment of Parkin (an ubiquitin ligase enzyme) to damaged or dysfunctional mitochondria (Filadi et al. 2018). Binding of Parkin to MFN2 via a PINK1 dependent manner can lead to mitophagy (Narendra et al. 2008; Narendra et al. 2010; Ding and Yin 2012). Our results showing significantly higher expression of Parkin upon ODE exposure support this explanation. In our study, a balance of mitochondrial fusion, along with fission leading to mitochondrial clearance could be the most probable scenario that could be occurring aimed at compensating for the cellular stress induced by ODE (Landes et al. 2010). Albeit no significant change in BNIP3 expression was observed upon exposure to ODE or ODE followed by EP compared to control, it was found to be significantly decreased in cells treated with ODE and MA. BNIP3, a transmembrane protein located in the OMM, imparts some pro-cell death activity and is known to regulate

mitophagy (Ney 2015). Addition of BNIP3 to isolated mitochondria has resulted in cytochrome c release, depolarization, and swelling (Kim et al. 2002). This phenomenon has been linked to BNIP3-mediated permeabilization of inner and outer mitochondrial membrane involving the disruption of OPA1 complex and remodeling of the inner mitochondrial membrane leading to cell death (Landes et al. 2010). Collectively, we can assume that MA-induced decrease in BNIP3 and OPA1 expression could be having a positive impact on the mitochondria and thus improving overall cellular function. Potential mechanism by which BNIP3 is promoting cell death is through competition for binding to Bcl-2 (or a related protein) which liberates Beclin-1 from Bcl-2 complexes and activates autophagy. Taken together we document a decrease in overall cell viability with ODE exposure which is rescued by co-treatment with MA indicating that cytoplasmic NOX2 inhibition is beneficial (Langley et al. 2017).

A prominent player in cell death is cytochrome c (Cai et al. 1998; Garrido et al. 2006). Cytochrome c, a peripheral protein of the mitochondrial inner membrane (IMM), is known to function as an electron shuttle between complex III and complex IV of the respiratory chain (Cai et al. 1998). Its activity and its release from the IMM has been implicated in caspase activation and mitochondrial outer membrane permeabilization (MOMP), leading to cell death (Garrido et al. 2006). In our findings, we observed that upon ODE exposure, there is an increase in cytosolic cytochrome c and a deficiency in the levels of COX4i2 (COX subunit 4 isoform 2), a terminal enzyme in the OXPHOS machinery. Loss of COX4i2 results in decreased COX activity and decreased ATP levels (Hüttemann et al. 2012). This loss is not reversed upon treatment with either EP or MA, albeit MA was capable of downregulating the release of cytochrome c. This is indicative that although antioxidant therapy can decrease the cytosolic release of cytochrome c, there could be other secondary factors promoting the loss of COX4i2. NADPH oxidase is the main source of ROS that is closely linked to mitochondrial ROS production (Zorov et al. 2014). It is known that presence of ROS can promote expression of pro-inflammatory mediators (Brand et al. 2004; Bhat et al. 2019). Treatment with MA brought the mitochondrial superoxide levels to that of control, whereas with ODE and EP co-treatment, it was significantly decreased. This could be a consequence of a leaky mitochondrial membrane enabling the release of superoxide ions into the cytosol thus promoting further damage to the cell. On the other hand, the increase in the SOD2 expression observed allows us to believe that there are factors possibly promoting the attenuation of oxidative stress mediated cellular injury through compensation. This increase could be due to the presence of factors, such as interleukin 1 (IL-1), IL-4, IL-6, tumor necrosis factor α, interferon γ, and the bacterial endotoxin lipopolysaccharide, which are considered to be robust SOD2 activators (Fukui and Zhu 2010). SOD2 is also said to be regulated by RNS, where increased peroxynitrite levels can lead to its enzymatic inhibition (Redondo-Horcajo et al. 2010). These antagonistic roles that peroxynitrite and superoxide radicals have in regulating SOD2 expression and activity leads us to believe that mitochondrial antioxidant response is dysregulated.

A consequence of leaky mitochondrial membrane during mitochondrial dysfunction is the release of mtDAMPs (Nakahira et al. 2011). Mitochondrial transcription factor A (mtTFA) is an integral regulator of mtDNA integrity, which, when released from mitochondria, acts as a mtDAMP to regulate inflammatory responses (Julian et al. 2013). Release of mtTFA along

with mtDNA during cell damage amplifies TNFα and type 1 interferon release, which plays a critical role in promoting sterile inflammation and autoimmune diseases (Cantaert et al. 2010; CHAUNG et al. 2012; Julian et al. 2012). This is in line with our findings where we observe an increase in the cytosolic release of mtTFA and mtDNA on ODE exposure. Although EP or MA therapy did not have a significant impact in reducing the release of mtTFA, it did however decrease the release of mtDNA into the cytosol. Since HMGB1 is a homolog of mtTFA (Parisi and Clayton 1991), we investigated whether it translocates from the normal nuclear location into the mitochondria in ODE exposed cells. Under pathophysiological conditions such as necrosis or inflammation, nuclear HMGB1 is immediately transported to the cytoplasm and released into the extracellular space where it acts as a signaling molecule regulating a wide range of inflammatory responses (Ugrinova and Pasheva 2017; Bhat et al. 2019). In endothelial cells, the translocation of endogenous HMGB1 from the nucleus to the mitochondria promotes mitochondrial reorganization (Stumbo et al. 2008; Hyun et al. 2016). Therefore, it is likely that the nuclear HMGB1 export would be involved the compensatory responses for maintenance of mitochondrial functions. However, in the present study we see that treatment with MA does not revert the levels of HMGB1 within the mitochondria and match the levels observed in controls.

Mitochondria are also key regulators of calcium (Ca^{2+}) which control a diverse range of cellular processes, including ROS production. Any aberrant increase in cytosolic Ca^{2+} and resultant $[Ca^{2+}]_{mito}$ overload can trigger cell death (Finkel et al. 2015). This overload has also been linked to induction increased permeabilization of mitochondrial membrane (Hunter et al. 1976; Finkel et al. 2015). This is corroborated by our findings where we observed $[Ca^{2+}]_{mito}$ levels on OD exposure. However, it could be possible that Ca^{2+} influx could possibly be occurring via the interaction of voltage-dependent anion channel (VDAC) with Mcl-1, a Bcl-2 family protein due to the decrease in Bcl-XL observed (Huang et al. 2014). Ca^{2+} signaling also plays a critical role in the activation of NLRP3 inflammasome by multiple stimuli (Murakami et al. 2012). This is corroborated by our data showing caspase-1 activation along with the increase in Ca^{2+} levels on ODE exposure (Yu et al. 2014). This would in turn lead to IL-1β activation and release into the extracellular space. The treatment with MA does not seem to have any impact on the levels of Ca^{2+} accumulation within the mitochondria.

Conclusion

In conclusion, we document that co-treatment with EP and MA are partially protective as they rescue some of the ODE-exposure induced mitochondrial deficits. However, our findings may lead to new questions on how ODE exposure may be causing mitochondrial dysfunction and cell death. Although our current study is limited to using a single immortalized cell line as a model, we report preliminary data on the impact of ODE exposure on mitochondrial biogenesis and function. Future studies using functional (primary alveolar macrophages, precision-cut lung slices) and mouse models would help us to unravel further underlying mechanisms.

Supplementary Material

Refer to Web version on PubMed Central for supplementary material.

Acknowledgments

We would like to thank Tracey Stewart at Iowa State University's Roy J. Carver High Resolution Microscopy Facility for assistance with transmission electron microscopy.

Funding

C.C. laboratory is funded through startup grant through Iowa State University and a pilot grant (5 U54 OH007548) from CDC-NIOSH (Centers for Disease Control and Prevention-The National Institute for Occupational Safety and Health). A.G.K. laboratory is supported by National Institutes of Health grants (ES026892, ES027245 and NS100090).

Abbreviations

OD	Organic Dust
ODE	Orgaic Dust Extract
EP	Ethyl Pyruvate
MA	Mitoapocynin
LPS	Lipopolysaccharide
PGN	Peptidoglycan
PAMPs	Pathogen Associated Molecular Patterns
COPD	Chronic Obstructive Pulmonary Disease
AHR	Airway hyperresponsiveness
ROS	Reactive Oxygen Species
RNS	Reactive Nitrogen Species
ATP	Adenosine Triphosphate
OXPHOS	Oxidative Phosphorylation
HMGB1	High Mobility Group Box 1
STAT	Signal Transducer and Activator of Transcription
TPP	Triphenylphosphonium
MPTP	1-Methyl-4-Phenyl-1,2,3,6-Tetrahydropyridine
iNOS	inducible Nitric Oxide Synthase
NOX	NADPH Oxidase
MTT	3-[4,5-dimethylthiazole-2-yl]-2,5-diphenyltetrazolium bromide

TEM	Transmission Electron Microscopy
DMSO	Dimethyl Sulfoxide
mtND1	mitochondrial NADH dehydrogenase 1
MFN	Mitofusin
OPA1	Optic Atrophy 1
DRP1	Dynamin-related protein 1
ER	Endoplasmic Reticulum
PINK1	PTEN- induced kinase 1
BNIP3	Bcl-2 Homology 3 (BH3)-only
MPT	Mitochondrial Permeability Transition
COX4i2	Cytochrome C Oxidase subunit 4 isoform 2
ETC	Electron Transport Chain
SOD2	Superoxide Dismutase 2
mtDAMPs	mitochondrial Damage Associated Molecular Patters
mtTFA	mitochondrial Transcription Factor A
MGC	Multinucleated Giant Cell
FBR	Foreign Body Reactions
OMM	Outer Mitochondrial Membrane
IMM	Inner Mitochondrial Membrane
IMS	Intermembrane Space
IL	Interleukin
cGAS	cyclic GMP-AMP synthase
TLR	Toll-like receptor
RAGE	Receptor for advanced glycation end products
VDAC	Voltage-dependent anion channel

References

Anantharam V, Kaul S, Song C, Kanthasamy A, Kanthasamy AG (2007) Pharmacological Inhibition of Neuronal NADPH Oxidase Protects against 1-Methyl-4-Phenylpyridinium (MPP+)-Induced Oxidative Stress and Apoptosis in Mesencephalic Dopaminergic Neuronal Cells. Neurotoxicology 28(5):988–997. 10.1016/j.neuro.2007.08.008 [PubMed: 17904225]

Bhat SM, Massey N, Karriker LA, Singh B, Charavaryamath C (2019) Ethyl pyruvate reduces organic dust-induced airway inflammation by targeting HMGB1-RAGE signaling. Respiratory Research 20(1):27. 10.1186/s12931-019-0992-3 [PubMed: 30728013]

Brand MD, Affourtit C, Esteves TC, Green K, Lambert AJ, Miwa S, Pakay JL, Parker N (2004) Mitochondrial superoxide: production, biological effects, and activation of uncoupling proteins. Free Radical Biology and Medicine 37(6):755–767. 10.1016/j.freeradbiomed.2004.05.034 [PubMed: 15304252]

Cai J, Yang J, Jones DeanP (1998) Mitochondrial control of apoptosis: the role of cytochrome c. Biochimica et Biophysica Acta (BBA) - Bioenergetics 1366(1):139–149. 10.1016/S0005-2728(98)00109-1 [PubMed: 9714780]

Cantaert T, Baeten D, Tak PP, van Baarsen LG (2010) Type I IFN and TNFα cross-regulation in immune-mediated inflammatory disease: basic concepts and clinical relevance. Arthritis Research & Therapy 12(5):219. 10.1186/ar3150 [PubMed: 21062511]

Charavaryamath C, Janardhan KS, Townsend HG, Willson P, Singh B (2005) Multiple exposures to swine barn air induce lung inflammation and airway hyper-responsiveness. Respiratory Research 6(1):50. 10.1186/1465-9921-6-50 [PubMed: 15932644]

Charavaryamath C, Juneau V, Suri SS, Janardhan KS, Townsend H, Singh B (2008) Role of Toll-like receptor 4 in lung inflammation following exposure to swine barn air. Exp Lung Res 34(1):19–35. 10.1080/01902140701807779 [PubMed: 18205075]

Charavaryamath C, Singh B (2006) Pulmonary effects of exposure to pig barn air. J Occup Med Toxicol 1:10. 10.1186/1745-6673-1-10 [PubMed: 16756675]

CHAUNG WW, WU R, JI Y, DONG W, WANG P (2012) Mitochondrial transcription factor A is a proinflammatory mediator in hemorrhagic shock. Int J Mol Med 30(1):199–203. 10.3892/ijmm.2012.959 [PubMed: 22469910]

Cloonan SM, Choi AM (2012) Mitochondria: commanders of innate immunity and disease? Current Opinion in Immunology 24(1):32–40. 10.1016/j.coi.2011.11.001 [PubMed: 22138315]

Cloonan SM, Choi AMK (2016) Mitochondria in lung disease. J Clin Invest 126(3):809–820. 10.1172/JCI81113 [PubMed: 26928034]

Cole D, Todd L, Wing S (2000) Concentrated swine feeding operations and public health: a review of occupational and community health effects. Environ Health Perspect 108(8):685–699

Cristóvão AC, Choi D-H, Baltazar G, Beal MF, Kim Y-S (2009) The Role of NADPH Oxidase 1–Derived Reactive Oxygen Species in Paraquat-Mediated Dopaminergic Cell Death. Antioxid Redox Signal 11(9):2105–2118. 10.1089/ars.2009.2459 [PubMed: 19450058]

Ding W-X, Yin X-M (2012) Mitophagy: mechanisms, pathophysiological roles, and analysis. Biol Chem 393(7):547–564. 10.1515/hsz-2012-0119 [PubMed: 22944659]

Eisner V, Picard M, Hajnóczky G (2018) Mitochondrial dynamics in adaptive and maladaptive cellular stress responses. Nature Cell Biology 20(7):755–765. 10.1038/s41556-018-0133-0 [PubMed: 29950571]

Fetterman JL, Sammy MJ, Ballinger SW (2017) Mitochondrial Toxicity of Tobacco Smoke and Air Pollution. Toxicology 391:18–33. 10.1016/j.tox.2017.08.002 [PubMed: 28838641]

Filadi R, Pendin D, Pizzo P (2018) Mitofusin 2: from functions to disease. Cell Death Dis 9(3):330. 10.1038/s41419-017-0023-6 [PubMed: 29491355]

Finkel T, Menazza S, Holmström KM, Parks RJ, Liu J, Sun J, Liu J, Pan X, Murphy E (2015) The Ins and Outs of Mitochondrial Calcium. Circ Res 116(11):1810–1819. 10.1161/CIRCRESAHA.116.305484 [PubMed: 25999421]

Fukui M, Zhu BT (2010) Mitochondrial Superoxide Dismutase SOD2, but not Cytosolic SOD1, Plays a Critical Role in Protection against Glutamate-Induced Oxidative Stress and Cell Death in HT22 Neuronal Cells. Free Radic Biol Med 48(6):821–830. 10.1016/j.freeradbiomed.2009.12.024 [PubMed: 20060889]

Garrido C, Galluzzi L, Brunet M, Puig PE, Didelot C, Kroemer G (2006) Mechanisms of cytochrome c release from mitochondria. Cell Death & Differentiation 13(9):1423–1433. 10.1038/sj.cdd.4401950 [PubMed: 16676004]

Ghosh A, Langley MR, Harischandra DS, Neal ML, Jin H, Anantharam V, Joseph J, Brenza T, Narasimhan B, Kanthasamy A, Kalyanaraman B, Kanthasamy AG (2016) Mitoapocynin

Treatment Protects Against Neuroinflammation and Dopaminergic Neurodegeneration in a Preclinical Animal Model of Parkinson's Disease. J Neuroimmune Pharmacol 11(2):259–278. 10.1007/s11481-016-9650-4 [PubMed: 26838361]

Gong Z, Pan J, Shen Q, Li M, Peng Y (2018) Mitochondrial dysfunction induces NLRP3 inflammasome activation during cerebral ischemia/reperfusion injury. Journal of Neuroinflammation 15(1):242. 10.1186/s12974-018-1282-6 [PubMed: 30153825]

Gordon R, Hogan CE, Neal ML, Anantharam V, Kanthasamy AG, Kanthasamy A (2011) A simple magnetic separation method for high-yield isolation of pure primary microglia. J Neurosci Methods 194(2):287–296. 10.1016/j.jneumeth.2010.11.001 [PubMed: 21074565]

Huang H, Shah K, Bradbury NA, Li C, White C (2014) Mcl-1 promotes lung cancer cell migration by directly interacting with VDAC to increase mitochondrial Ca 2+ uptake and reactive oxygen species generation. Cell Death & Disease 5(10):e1482–e1482. 10.1038/cddis.2014.419 [PubMed: 25341036]

Hunter DR, Haworth RA, Southard JH (1976) Relationship between configuration, function, and permeability in calcium-treated mitochondria. J Biol Chem 251(16):5069–5077 [PubMed: 134035]

Hüttemann M, Lee I, Gao X, Pecina P, Pecinova A, Liu J, Aras S, Sommer N, Sanderson TH, Tost M, Neff F, Aguilar-Pimentel JA, Becker L, Naton B, Rathkolb B, Rozman J, Favor J, Hans W, Prehn C, Puk O, Schrewe A, Sun M, Höfler H, Adamski J, Bekeredjian R, Graw J, Adler T, Busch DH, Klingenspor M, Klopstock T, Ollert M, Wolf E, Fuchs H, Gailus-Durner V, de Angelis MH, Weissmann N, Doan JW, Bassett DJP, Grossman LI (2012) Cytochrome c oxidase subunit 4 isoform 2-knockout mice show reduced enzyme activity, airway hyporeactivity, and lung pathology. The FASEB Journal 26(9):3916–3930. 10.1096/fj.11-203273 [PubMed: 22730437]

Hyun H-W, Ko A-R, Kang T-C (2016) Mitochondrial Translocation of High Mobility Group Box 1 Facilitates LIM Kinase 2-Mediated Programmed Necrotic Neuronal Death. Front Cell Neurosci 10. 10.3389/fncel.2016.00099

Ishihara Y, Takemoto T, Itoh K, Ishida A, Yamazaki T (2015) Dual Role of Superoxide Dismutase 2 Induced in Activated Microglia OXIDATIVE STRESS TOLERANCE AND CONVERGENCE OF INFLAMMATORY RESPONSES. J Biol Chem 290(37):22805–22817. 10.1074/jbc.M115.659151 [PubMed: 26231211]

Julian MW, Shao G, Bao S, Knoell DL, Papenfuss TL, VanGundy ZC, Crouser ED (2012) Mitochondrial Transcription Factor A Serves as a Danger Signal by Augmenting Plasmacytoid Dendritic Cell Responses to DNA. The Journal of Immunology 189(1):433–443. 10.4049/jimmunol.1101375 [PubMed: 22675199]

Julian MW, Shao G, Vangundy ZC, Papenfuss TL, Crouser ED (2013) Mitochondrial transcription factor A, an endogenous danger signal, promotes TNFα release via RAGE- and TLR9-responsive plasmacytoid dendritic cells. PLoS ONE 8(8):e72354. 10.1371/journal.pone.0072354 [PubMed: 23951313]

Kelly B, O'Neill LA (2015) Metabolic reprogramming in macrophages and dendritic cells in innate immunity. Cell Research 25(7):771–784. 10.1038/cr.2015.68 [PubMed: 26045163]

Kim HS, Cho IH, Kim JE, Shin YJ, Jeon J-H, Kim Y, Yang YM, Lee K-H, Lee JW, Lee W-J, Ye S-K, Chung M-H (2008) Ethyl pyruvate has an anti-inflammatory effect by inhibiting ROS-dependent STAT signaling in activated microglia. Free Radic Biol Med 45(7):950–963. 10.1016/j.freeradbiomed.2008.06.009 [PubMed: 18625301]

Kim J-Y, Cho J-J, Ha J, Park J-H (2002) The Carboxy Terminal C-Tail of BNip3 Is Crucial in Induction of Mitochondrial Permeability Transition in Isolated Mitochondria. Archives of Biochemistry and Biophysics 398(2):147–152. 10.1006/abbi.2001.2673 [PubMed: 11831844]

Krysko DV, Denecker G, Festjens N, Gabriels S, Parthoens E, D'Herde K, Vandenabeele P (2006) Macrophages use different internalization mechanisms to clear apoptotic and necrotic cells. Cell Death & Differentiation 13(12):2011–2022. 10.1038/sj.cdd.4401900 [PubMed: 16628234]

Landes T, Emorine LJ, Courilleau D, Rojo M, Belenguer P, Arnauné-Pelloquin L (2010) The BH3-only Bnip3 binds to the dynamin Opa1 to promote mitochondrial fragmentation and apoptosis by distinct mechanisms. EMBO reports 11(6):459–465. 10.1038/embor.2010.50 [PubMed: 20436456]

Langley M, Ghosh A, Charli A, Sarkar S, Ay M, Luo J, Zielonka J, Brenza T, Bennett B, Jin H, Ghaisas S, Schlichtmann B, Kim D, Anantharam V, Kanthasamy A, Narasimhan B, Kalyanaraman B, Kanthasamy AG (2017) Mito-Apocynin Prevents Mitochondrial Dysfunction, Microglial

Activation, Oxidative Damage, and Progressive Neurodegeneration in MitoPark Transgenic Mice. Antioxidants & Redox Signaling 27(14):1048–1066. 10.1089/ars.2016.6905 [PubMed: 28375739]

Latchoumycandane C, Anantharam V, Kitazawa M, Yang Y, Kanthasamy A, Kanthasamy AG (2005) Protein kinase Cdelta is a key downstream mediator of manganese-induced apoptosis in dopaminergic neuronal cells. J Pharmacol Exp Ther 313(1):46–55. 10.1124/jpet.104.078469 [PubMed: 15608081]

Liu J, Fang H, Chi Z, Wu Z, Wei D, Mo D, Niu K, Balajee AS, Hei TK, Nie L, Zhao Y (2015) XPD localizes in mitochondria and protects the mitochondrial genome from oxidative DNA damage. Nucleic Acids Res 43(11):5476–5488. 10.1093/nar/gkv472 [PubMed: 25969448]

Livak KJ, Schmittgen TD (2001) Analysis of Relative Gene Expression Data Using Real-Time Quantitative PCR and the 2−ΔΔCT Method. Methods 25(4):402–408. 10.1006/meth.2001.1262 [PubMed: 11846609]

Massey N, Puttachary S, Bhat SM, Kanthasamy AG, Charavaryamath C (2019) HMGB1-RAGE Signaling Plays a Role in Organic Dust-Induced Microglial Activation and Neuroinflammation. Toxicol Sci 169(2):579–592. 10.1093/toxsci/kfz071 [PubMed: 30859215]

May S, Romberger DJ, Poole JA (2012) Respiratory Health Effects of Large Animal Farming Environments. J Toxicol Environ Health B Crit Rev 15(8):524–541. 10.1080/10937404.2012.744288 [PubMed: 23199220]

Mishra P, Chan DC (2014) Mitochondrial dynamics and inheritance during cell division, development and disease. Nature Reviews Molecular Cell Biology 15(10):634–646. 10.1038/nrm3877 [PubMed: 25237825]

Murakami T, Ockinger J, Yu J, Byles V, McColl A, Hofer AM, Horng T (2012) Critical role for calcium mobilization in activation of the NLRP3 inflammasome. Proc Natl Acad Sci USA 109(28):11282–11287. 10.1073/pnas.1117765109 [PubMed: 22733741]

Nakahira K, Haspel JA, Rathinam VAK, Lee S-J, Dolinay T, Lam HC, Englert JA, Rabinovitch M, Cernadas M, Kim HP, Fitzgerald KA, Ryter SW, Choi AMK (2011) Autophagy proteins regulate innate immune responses by inhibiting the release of mitochondrial DNA mediated by the NALP3 inflammasome. Nature Immunology 12(3):222–230. 10.1038/ni.1980 [PubMed: 21151103]

Narendra D, Tanaka A, Suen D-F, Youle RJ (2008) Parkin is recruited selectively to impaired mitochondria and promotes their autophagy. J Cell Biol 183(5):795–803. 10.1083/jcb.200809125 [PubMed: 19029340]

Narendra DP, Jin SM, Tanaka A, Suen D-F, Gautier CA, Shen J, Cookson MR, Youle RJ (2010) PINK1 Is Selectively Stabilized on Impaired Mitochondria to Activate Parkin. PLOS Biology 8(1):e1000298. 10.1371/journal.pbio.1000298 [PubMed: 20126261]

Nath Neerukonda S, Mahadev-Bhat S, Aylward B, Johnson C, Charavaryamath C, Arsenault RJ (2018) Kinome analyses of inflammatory responses to swine barn dust extract in human bronchial epithelial and monocyte cell lines. Innate Immun 24(6):366–381. 10.1177/1753425918792070 [PubMed: 30092684]

Ney PA (2015) Mitochondrial autophagy: Origins, significance, and role of BNIP3 and NIX. Biochimica et Biophysica Acta (BBA) - Molecular Cell Research 1853(10, Part B):2775–2783. 10.1016/j.bbamcr.2015.02.022 [PubMed: 25753537]

Nordgren TM, Charavaryamath C (2018) Agriculture Occupational Exposures and Factors Affecting Health Effects. Curr Allergy Asthma Rep 18(12):65. 10.1007/s11882-018-0820-8 [PubMed: 30291457]

Parisi MA, Clayton DA (1991) Similarity of human mitochondrial transcription factor 1 to high mobility group proteins. Science 252(5008):965–969. 10.1126/science.2035027 [PubMed: 2035027]

Picard M, White K, Turnbull DM (2013) Mitochondrial morphology, topology, and membrane interactions in skeletal muscle: a quantitative three-dimensional electron microscopy study. J Appl Physiol (1985) 114(2):161–171. 10.1152/japplphysiol.01096.2012 [PubMed: 23104694]

Poole JA, Burrell AM, Wyatt TA, Kielian TL, Romberger DJ (2010) NOD2 Negatively Regulates Organic Dust-Induced Inflammation in Monocytes/Macrophages. Journal of Allergy and Clinical Immunology 125(2, Supplement 1):AB118. 10.1016/j.jaci.2009.12.467

Poole JA, Wyatt TA, Kielian T, Oldenburg P, Gleason AM, Bauer A, Golden G, West WW, Sisson JH, Romberger DJ (2011) Toll-like receptor 2 regulates organic dust-induced airway inflammation. Am J Respir Cell Mol Biol 45(4):711–719. 10.1165/rcmb.2010-0427OC [PubMed: 21278324]

Prakash YS, Pabelick CM, Sieck GC (2017) Mitochondrial Dysfunction in Airway Disease. CHEST 152(3):618–626. 10.1016/j.chest.2017.03.020 [PubMed: 28336486]

Qi L, Sun X, Li F-E, Zhu B-S, Braun FK, Liu Z-Q, Tang J-L, Wu C, Xu F, Wang H-H, Velasquez LA, Zhao K, Lei F-R, Zhang J-G, Shen Y-T, Zou J-X, Meng H-M, An G-L, Yang L, Zhang X-D (2015) HMGB1 Promotes Mitochondrial Dysfunction–Triggered Striatal Neurodegeneration via Autophagy and Apoptosis Activation. PLoS One 10(11). 10.1371/journal.pone.0142901

Redondo-Horcajo M, Romero N, Martínez-Acedo P, Martínez-Ruiz A, Quijano C, Lourenço CF, Movilla N, Enríquez JA, Rodríguez-Pascual F, Rial E, Radi R, Vázquez J, Lamas S (2010) Cyclosporine A-induced nitration of tyrosine 34 MnSOD in endothelial cells: role of mitochondrial superoxide. Cardiovasc Res 87(2):356–365. 10.1093/cvr/cvq028 [PubMed: 20106845]

Romberger DJ, Bodlak V, Von Essen SG, Mathisen T, Wyatt TA (2002) Hog barn dust extract stimulates IL-8 and IL-6 release in human bronchial epithelial cells via PKC activation. Journal of Applied Physiology 93(1):289–296. 10.1152/japplphysiol.00815.2001 [PubMed: 12070216]

Sahlander K, Larsson K, Palmberg L (2012) Daily exposure to dust alters innate immunity. PLoS ONE 7(2):e31646. 10.1371/journal.pone.0031646 [PubMed: 22355383]

Sethi RS, Schneberger D, Charavaryamath C, Singh B (2017) Pulmonary innate inflammatory responses to agricultural occupational contaminants. Cell Tissue Res 367(3):627–642. 10.1007/s00441-017-2573-4 [PubMed: 28168324]

Shin J-H, Kim I-D, Kim S-W, Lee H-K, Jin Y, Park J-H, Kim T-K, Suh C-K, Kwak J, Lee K-H, Han P-L, Lee J-K (2014) Ethyl Pyruvate Inhibits HMGB1 Phosphorylation and Release by Chelating Calcium. Mol Med 20(1):649–657. 10.2119/molmed.2014.00039

Stefanska J, Pawliczak R (2008) Apocynin: Molecular Aptitudes. Mediators of Inflammation 2008:1–10. 10.1155/2008/106507

Stumbo AC, Cortez E, Rodrigues CA, Henriques M das GMO, Porto LC, Barbosa HS, Carvalho L (2008) Mitochondrial localization of non-histone protein HMGB1 during human endothelial cell–Toxoplasma gondii infection. Cell Biology International 32(2):235–238. 10.1016/j.cellbi.2007.08.031 [PubMed: 17936030]

Su Y, Zhu L, Yu X, Cai L, Lu Y, Zhang J, Li T, Li J, Xia J, Xu F, Hu Q (2016) Mitochondrial Transplantation Attenuates Airway Hyperresponsiveness by Inhibition of Cholinergic Hyperactivity. Theranostics 6(8):1244–1260. 10.7150/thno.13804 [PubMed: 27279915]

Tang D, Kang R, Livesey KM, Kroemer G, Billiar TR, Van Houten B, Zeh HJ, Lotze MT (2011) High-Mobility Group Box 1 Is Essential for Mitochondrial Quality Control. Cell Metabolism 13(6):701–711. 10.1016/j.cmet.2011.04.008 [PubMed: 21641551]

Tilokani L, Nagashima S, Paupe V, Prudent J (2018) Mitochondrial dynamics: overview of molecular mechanisms. Essays Biochem 62(3):341–360. 10.1042/EBC20170104 [PubMed: 30030364]

Ugrinova I, Pasheva E (2017) HMGB1 Protein: A Therapeutic Target Inside and Outside the Cell. Adv Protein Chem Struct Biol 107:37–76. 10.1016/bs.apcsb.2016.10.001 [PubMed: 28215228]

Venkataraman R, Kellum JA, Song M, Fink MP (2002) Resuscitation with Ringer's ethyl pyruvate solution prolongs survival and modulates plasma cytokine and nitrite/nitrate concentrations in a rat model of lipopolysaccharide-induced shock. Shock 18(6):507–512. 10.1097/00024382-200212000-00004 [PubMed: 12462557]

Vested A, Basinas I, Burdorf A, Elholm G, Heederik DJJ, Jacobsen GH, Kolstad HA, Kromhout H, Omland Ø, Sigsgaard T, Thulstrup AM, Toft G, Vestergaard JM, Wouters IM, Schlünssen V (2019) A nationwide follow-up study of occupational organic dust exposure and risk of chronic obstructive pulmonary disease (COPD). Occup Environ Med 76(2):105–113. 10.1136/oemed-2018-105323 [PubMed: 30598459]

Wai T, Langer T (2016) Mitochondrial Dynamics and Metabolic Regulation. Trends in Endocrinology & Metabolism 27(2):105–117. 10.1016/j.tem.2015.12.001 [PubMed: 26754340]

Westrate LM, Drocco JA, Martin KR, Hlavacek WS, MacKeigan JP (2014) Mitochondrial Morphological Features Are Associated with Fission and Fusion Events. PLOS ONE 9(4):e95265. 10.1371/journal.pone.0095265 [PubMed: 24733410]

Wunschel J, Poole JA (2016) Occupational agriculture organic dust exposure and its relationship to asthma and airway inflammation in adults. J Asthma 53(5):471–477. 10.3109/02770903.2015.1116089 [PubMed: 26785925]

Yu J, Nagasu H, Murakami T, Hoang H, Broderick L, Hoffman HM, Horng T (2014) Inflammasome activation leads to Caspase-1–dependent mitochondrial damage and block of mitophagy. Proc Natl Acad Sci U S A 111(43):15514–15519. 10.1073/pnas.1414859111 [PubMed: 25313054]

Yu Y-M, Kim J-B, Lee K-W, Kim SY, Han P-L, Lee J-K (2005) Inhibition of the cerebral ischemic injury by ethyl pyruvate with a wide therapeutic window. Stroke 36(10):2238–2243. 10.1161/01.STR.0000181779.83472.35 [PubMed: 16141417]

Zhang Q, Raoof M, Chen Y, Sumi Y, Sursal T, Junger W, Brohi K, Itagaki K, Hauser CJ (2010) Circulating mitochondrial DAMPs cause inflammatory responses to injury. Nature 464(7285):104–107. 10.1038/nature08780 [PubMed: 20203610]

Zorov DB, Juhaszova M, Sollott SJ (2014) Mitochondrial Reactive Oxygen Species (ROS) and ROS-Induced ROS Release. Physiol Rev 94(3):909–950. 10.1152/physrev.00026.2013 [PubMed: 24987008]

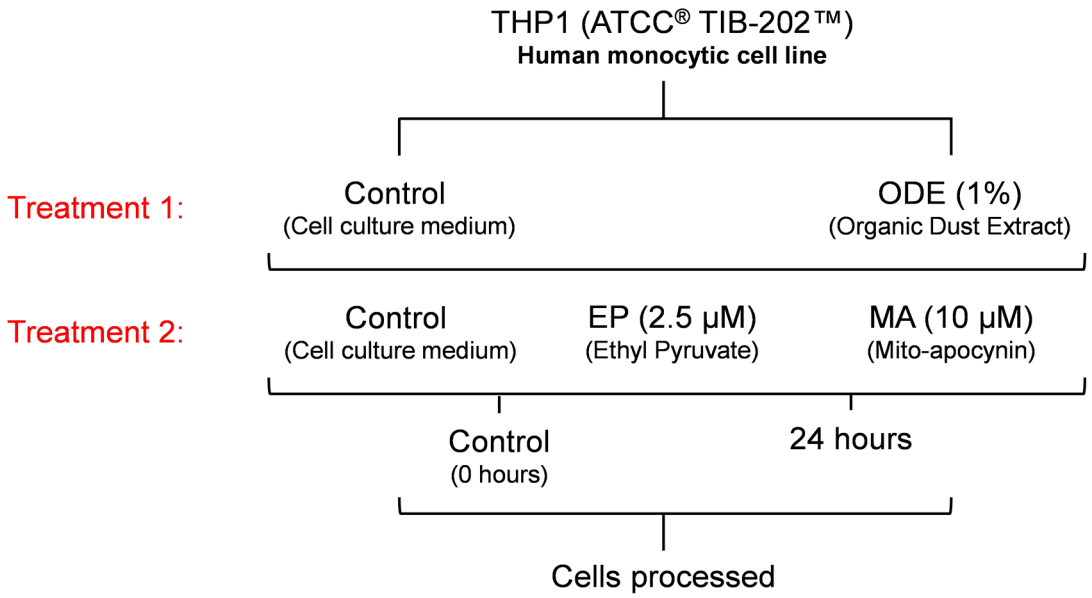

Fig. 1. ODE exposure of THP1 cells and antioxidant treatment.

THP1 cells were treated with either media (control) or ODE (treatment 1) followed by either media, EP or MA (treatment 2). Cells were processed for various assays at 0 (control), and 24 hours.

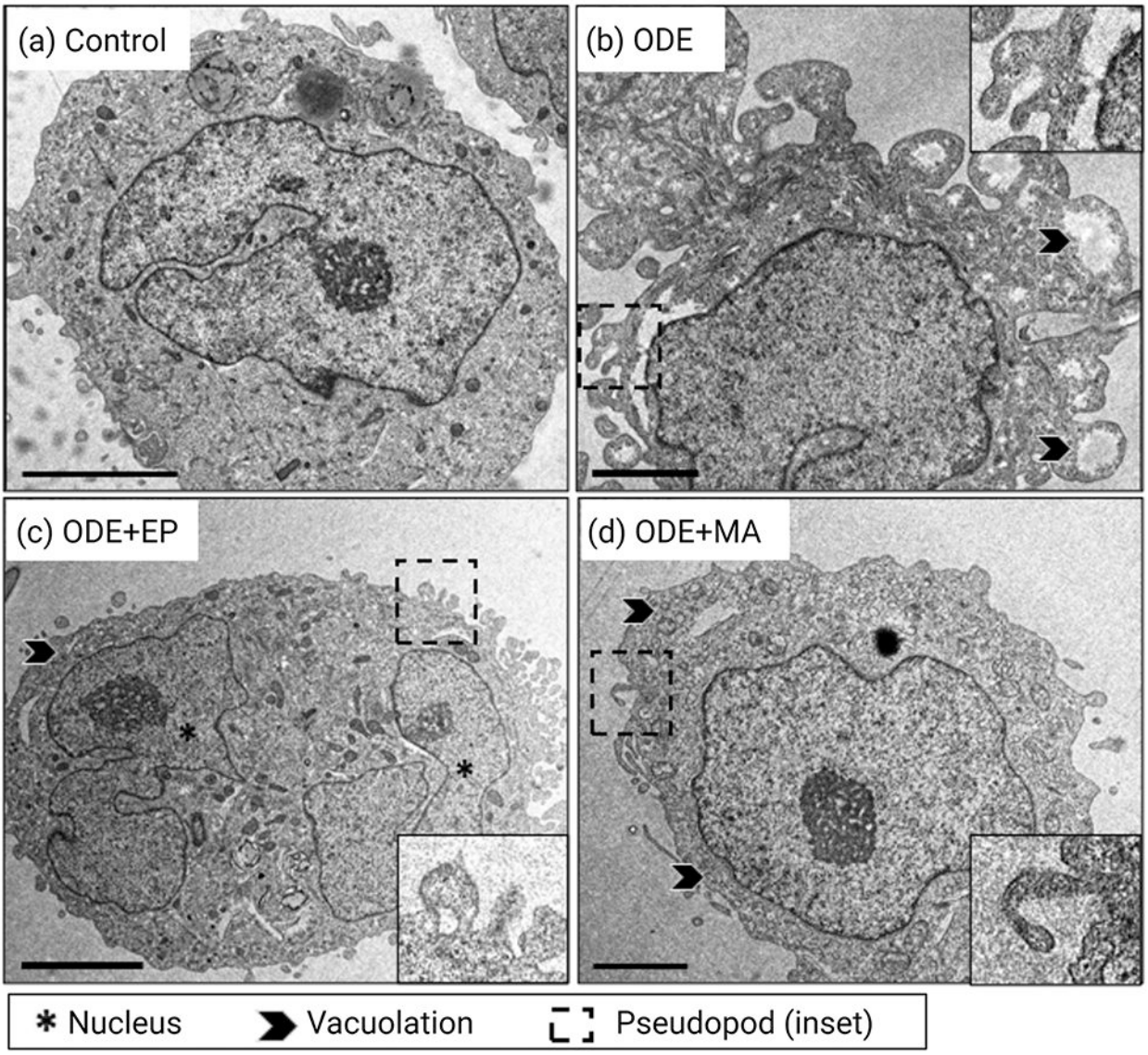

Fig. 2. ODE exposure induces differentiation of THP1 cells with ultrastructural changes to cellular morphology.

Transmission electron microscopy (TEM) of THP1 cells treated with medium or ODE (1%) followed by medium or EP (2.5 μM) or MA (10 μM) for 24 hours shows changes in cellular morphology at the ultrastructural level. Compared to controls, cells exposed to ODE differentiated into activated macrophages, with increased vacuolation and pseudopod formation (a-d, scale bar, 2-5 μm).

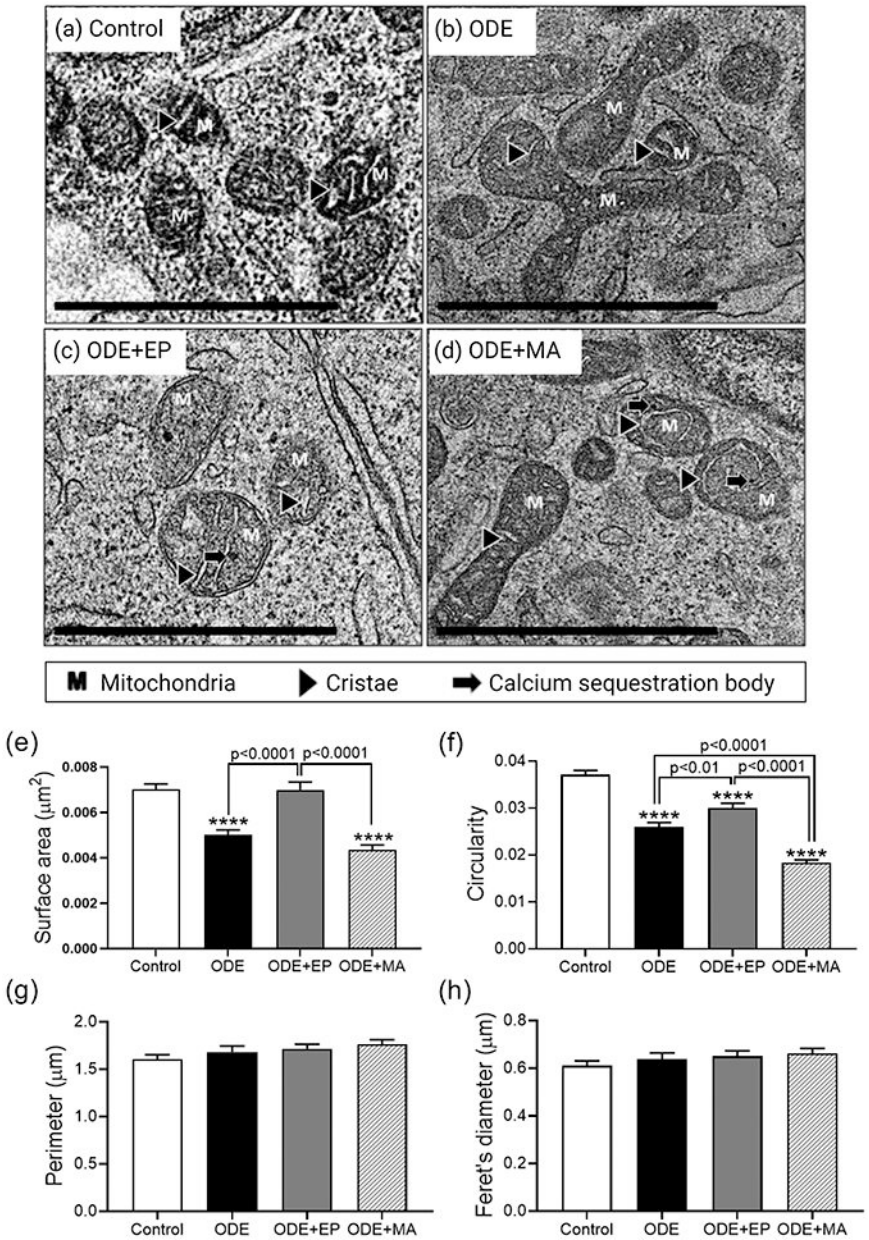

Fig. 3. ODE exposure induced changes in mitochondrial morphological features in THP1 cells.

Transmission electron microscopy (TEM) of THP1 cells treated with medium or ODE (1%) followed by medium or EP (2.5 μM) or MA (10 μM) for 24 hours show changes in the mitochondrial morphology. A number of mitochondria displayed changes in morphology (fission/fusion) and swelling (a-d, scale bar, 2-5 μm), along with presence of calcium sequestration bodies within the mitochondrial matrix in cells co-treated with of EP (2.5 μM). Cells treated with ODE followed by MA showed noticeably healthier mitochondria with a few morphological changes (fission/fusion). Morphological parameters of mitochondria of THP1 cells was analyzed by ImageJ (e-f). Measurement of surface area (e), circularity (f), perimeter (g) and Feret's diameter (h) of the mitochondria were determined. Data analyzed via one-way ANOVA with Tukey's multiple comparison test (*p < 0.05, **p < 0.01, ***p <

0.001, ****p < 0.0001) and are represented as Mean ± SEM with n = 126 mitochondria/ treatment (* indicates significant difference from control).

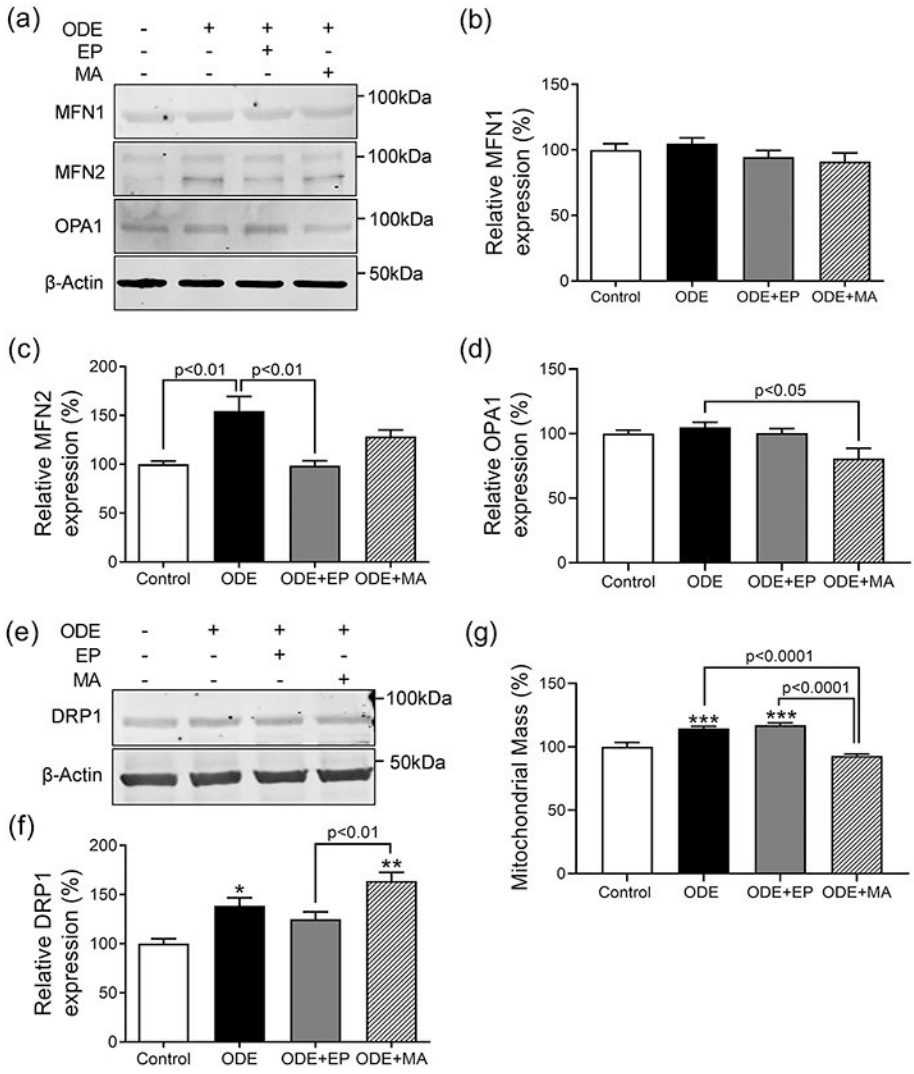

Fig. 4. ODE exposure induces fusion of mitochondria in response to stress.

Immunoblotting of whole-cell lysates of THP1 cells treated with medium or ODE (1%) followed by medium or EP (2.5 μM) or MA (10 μM) for 24 hours was performed to detect mitochondrial fusion proteins MFN1 (a,b), MFN2 (a,c) and OPA1 (a,d) and fission protein DRP1 (e,f) and compared. Mitochondrial mass was measured by staining with Mito-tracker dye (g). Samples for all assays were derived from the same experiment and were processed in parallel. All the protein bands were normalized over b-actin (37 kD) and percentage intensity relative to control was analyzed. Data was analyzed using one-way ANOVA with Tukey's multiple comparison test (*$p < 0.05$, **$p < 0.01$, ***$p < 0.001$, ****$p < 0.0001$) and represented as mean ± SEM with n = 3-6/treatment (* indicates significant difference from control).

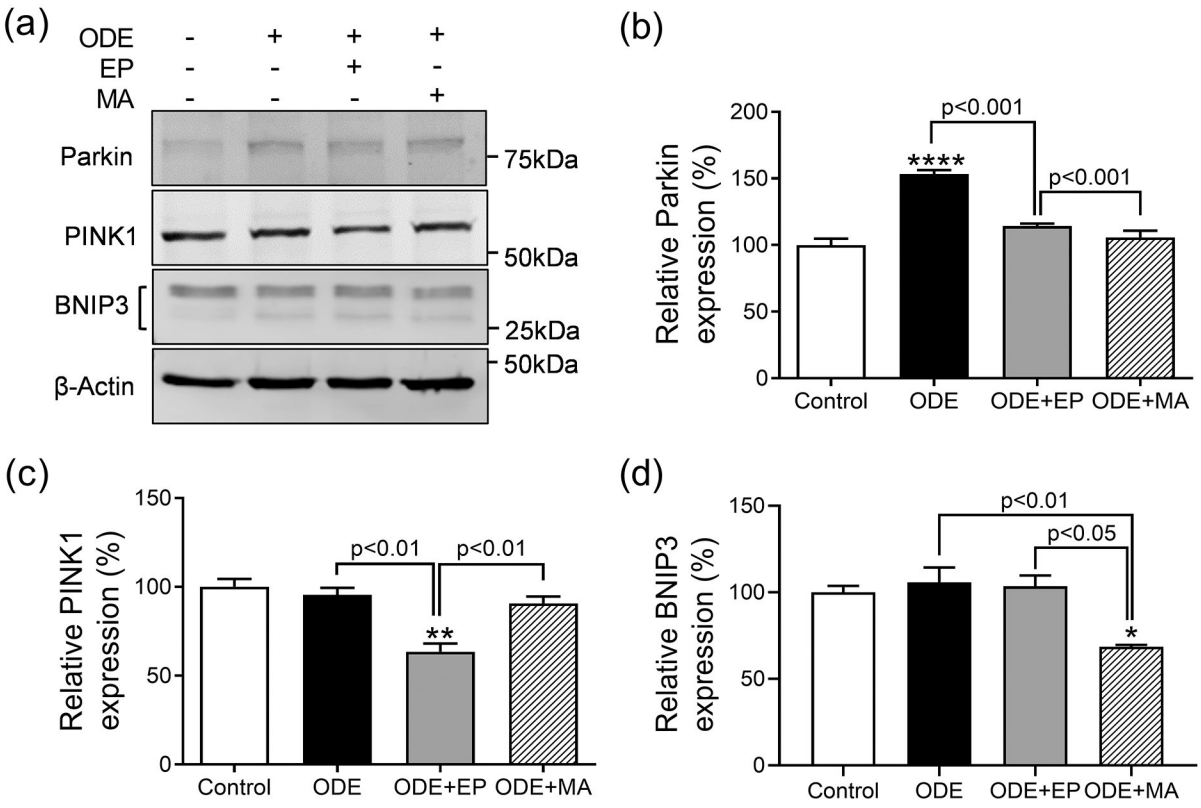

Fig. 5. ODE exposure induces selective targeting of mitochondria for autophagy (mitophagy).

Immunoblotting of whole-cell lysates of THP1 cells, treated with medium or ODE (1%) followed by either medium or EP (2.5 μM) or MA (10 μM) for 24 hours, was performed to detect expression of mitophagy markers, Parkin (a, b) and PINK1 (a, c), and BNIP3 (a, d). For all the western blots, samples were derived from the same experiment and were processed in parallel. All the protein bands were normalized over b-actin (37 kD) and percentage intensity relative to control was analyzed. Data was analyzed using one-way ANOVA with Tukey's multiple comparison test (*$p < 0.05$, **$p < 0.01$, ***$p < 0.001$, ****$p < 0.0001$) and represented as mean ± SEM with n = 3/treatment (* indicates significant difference from control).

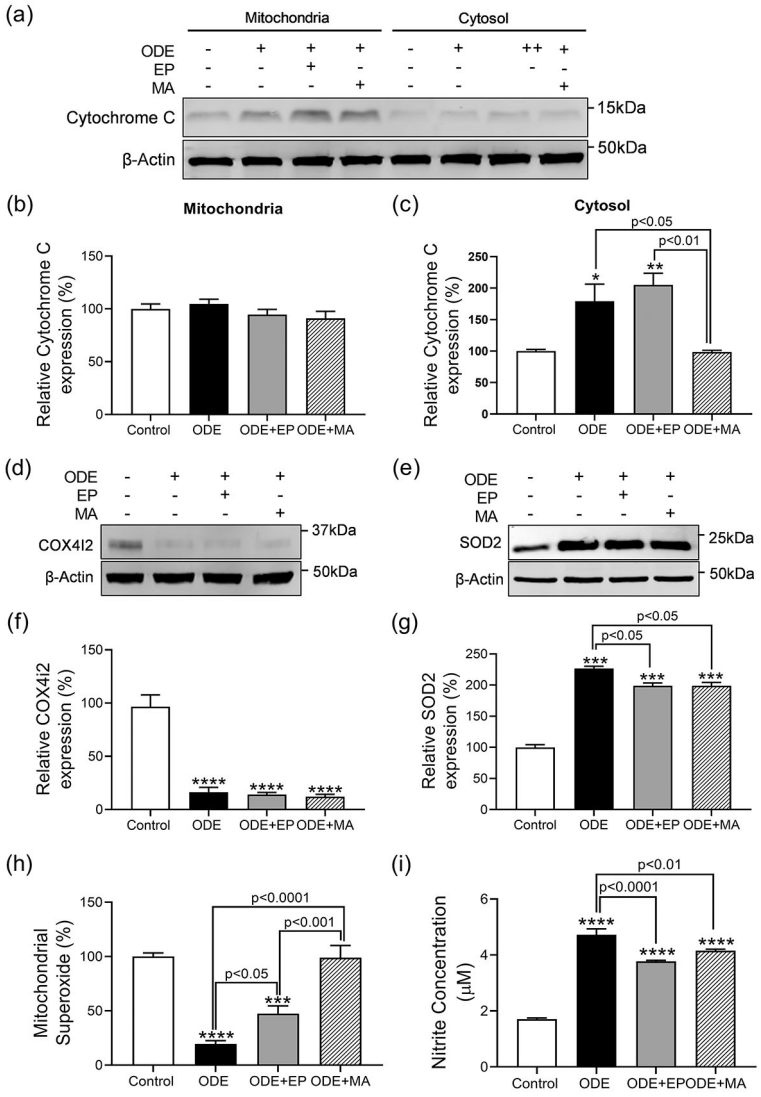

Fig. 6. Mitoapocyanin treatment decreases ODE-induced Cytochrome C release and markedly increases SOD2 expression in the cytosol.

We performed the immunoblotting of mitochondrial and mitochondria-free cytosolic fractions of THP1 cells, treated with medium or ODE (1%) followed by either medium or EP (2.5 μM) or MA (10 μM) for 24 hours, to detect the presence of Cytochrome C and expression of lung-specific isoform of COX, COX4i2, and SOD2. Cytochrome C expression was compared between the mitochondrial (a, b) and cytosolic (a, c) fractions of the cells. Measurement of expression of COX4i2 (d, f), and superoxide dismutase 2 (SOD2) (e, g) in the mitochondrial fractions of the treated cells was performed. Using the MitoSox and Griess assays, the levels of superoxide anions (SOX) (h) and secreted nitrites (i) were measured respectively. Samples for all assays were derived from the same experiment and were processed in parallel. All the protein bands were normalized over b-actin (37 kD) and percentage intensity relative to control analyzed. Data was analyzed using one-way ANOVA with Tukey's multiple comparison test (*p < 0.05, **p < 0.01, ***p < 0.001, ****p <

0.0001) and represented as mean ± SEM with n = 3-6/treatment (* indicates significant difference from control).

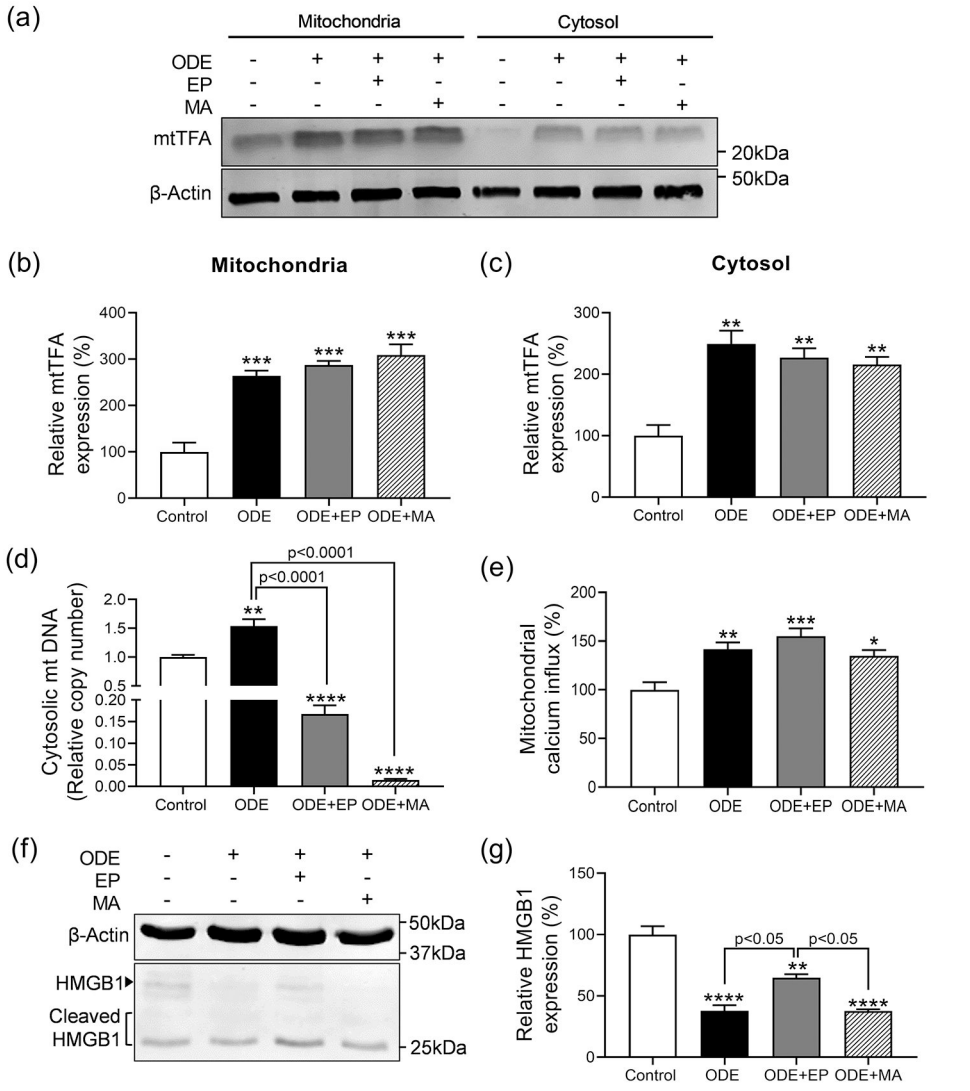

Fig. 7. ODE exposure markedly increases secretion of mitochondrial DAMPs into the cytosol.

Immunoblotting of mitochondrial and mitochondria-free cytosolic fractions of THP1 cells, treated with medium or ODE (1%) followed by either medium or EP (2.5 μM) or MA (10 μM) for 24 hours, was performed to detect expression of mitochondrial transcription factor activator (mtTFA) (a-c). mtTFA expression was compared in the mitochondrial (b) and cytosolic (c) fractions of the cells to assess leaky mitochondrial membrane. Mitochondrial DNA leakage into the cytosol was analyzed via qPCR (d). Intra-mitochondrial calcium levels in mitochondria isolated from the treated cells was measured by Rhod 2AM staining (e). Immunoblotting of mitochondrial fraction of THP1 cells was performed to measure HMGB1 expression in mitochondria (f, g). Samples for all assays were derived from the same experiment and were processed in parallel. All protein bands were normalized over b-actin (37 kD) and percentage intensity relative to control analyzed. Data was analyzed using one-way ANOVA with Tukey's multiple comparison test (*$p < 0.05$, **$p < 0.01$, ***$p < 0.001$, ****$p < 0.0001$) and represented as mean ± SEM with n = 3-6/treatment (* indicates significant difference from control).

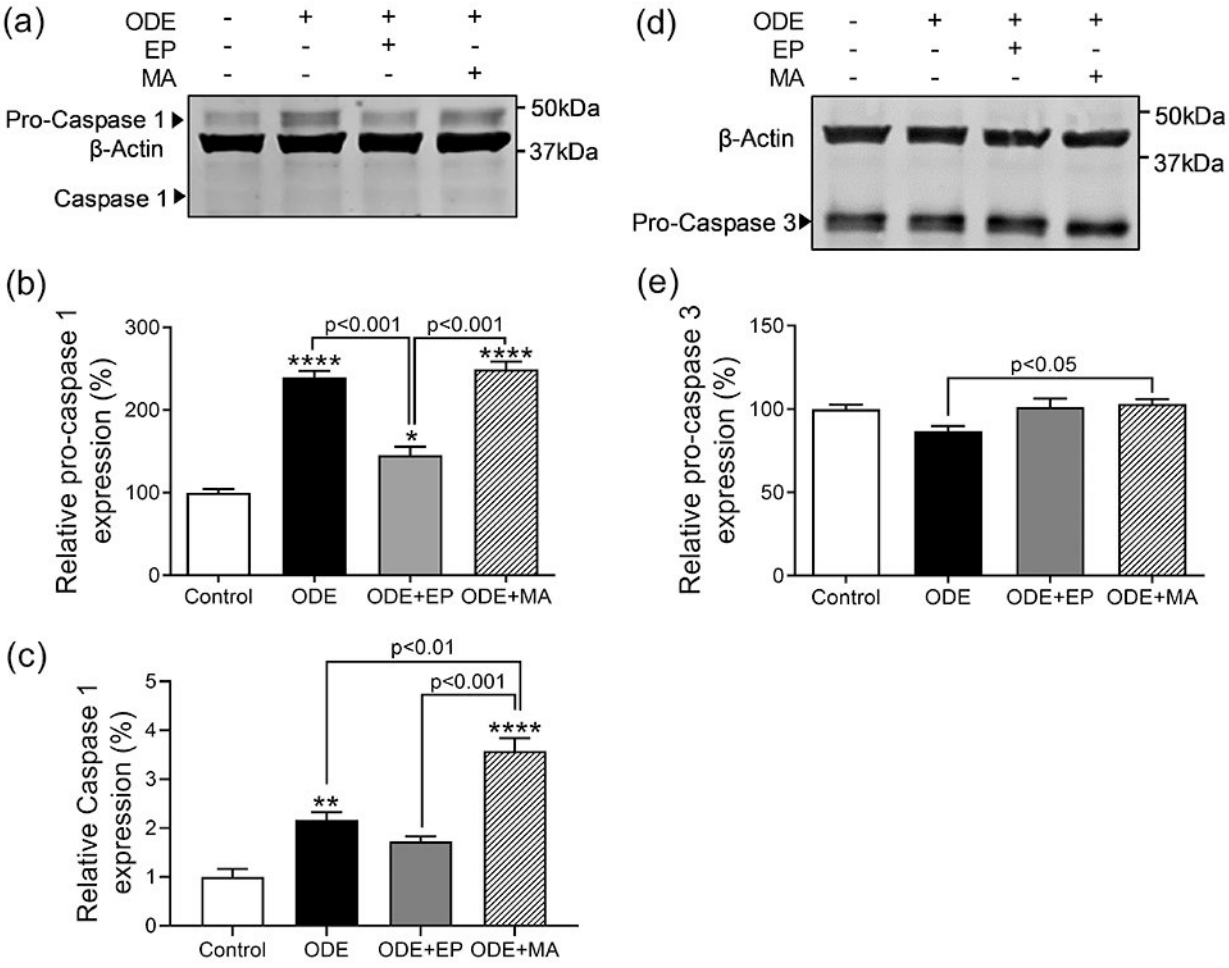

Fig. 8. ODE exposure increases expression of Caspase 1.

Immunoblotting of whole cell lysates of THP1 cells, treated with either medium or ODE (1%) followed by either medium or EP (2.5 μM) or MA (10 μM) for 24 hours was performed to detect the expression of caspase 1 and 3. Expression of pro-caspase 1 (a, b), along with the cleaved caspase 1 p10 (a, c) in treated cells was measured and compared. Expression of pro-caspase 3 in treated cells was measured (d, e). For all western blots, samples were derived from the same experiment and were processed in parallel. All protein bands were normalized over b-actin (37 kD) and percentage intensity relative to control was analyzed. Data was analyzed using one-way ANOVA with Tukey's multiple comparison test (*$p < 0.05$, **$p < 0.01$, ***$p < 0.001$, ****$p < 0.0001$) and represented as mean ± SEM with n = 3/treatment (* indicates significant difference from control).

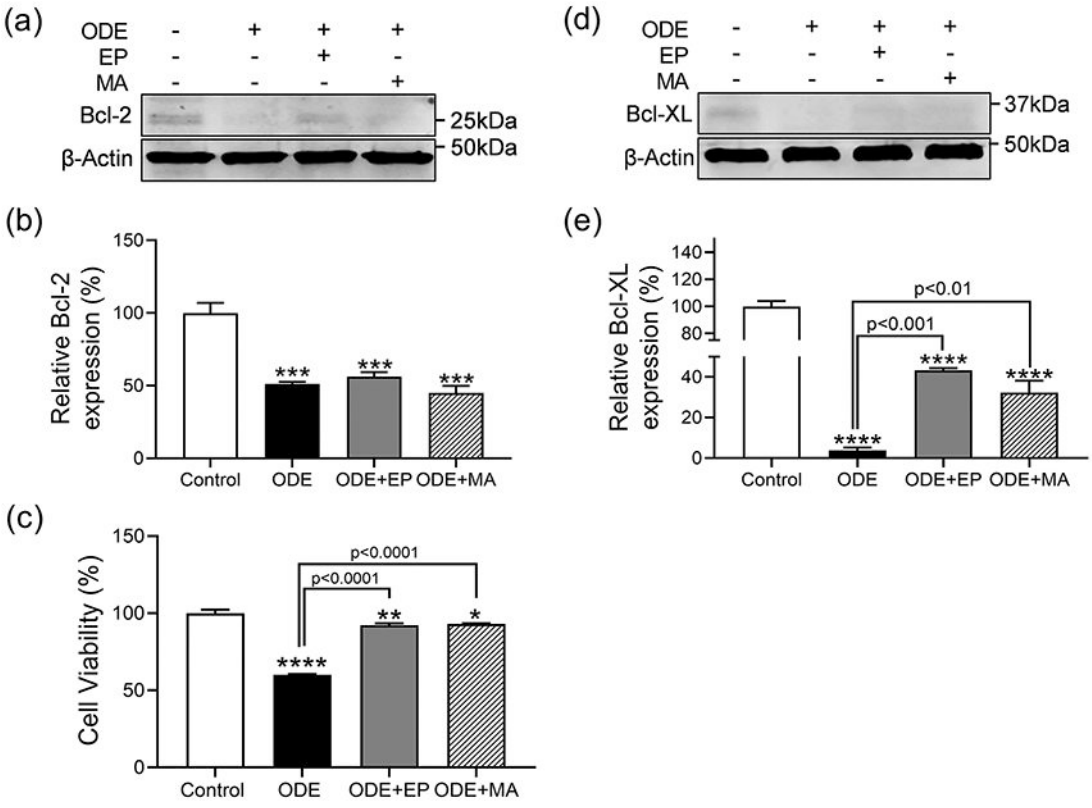

Fig. 9. Mitochondrial targeted antioxidant treatment has no effect Bcl-2 and Bcl-XL expression.

Immunoblotting of whole cell lysates of THP1 cells, treated with ODE (1%), EP (2.5 μM), or MA (10 μM) for 24 hours, was performed to observe expression of Bcl-2 (a, b) and Bcl-XL (d, e). MTT assay was performed to measure cell viability on treatment (c). Samples for all assays were derived from the same experiment and were processed in parallel. All protein bands were normalized over b-actin (37 kD) and percentage intensity relative to control analyzed. Data was analyzed using one-way ANOVA with Tukey's multiple comparison test (*p < 0.05, **p < 0.01, ***p < 0.001, ****p < 0.0001) and represented as Mean ± SEM with n = 3-6/treatment (* indicates different from control).

Table 1

Characteristics of primary antibodies

Epitope	Species/Clone	Dilution	Catalog #	Supplier
β-Actin	Mouse Monoclonal	1:10,000	ab6276	AbCam[a]
HMGB1	Rabbit Polyclonal	1:5000	ab79823	AbCam[a]
MFN1	Mouse Monoclonal	1:1000	sc-166644	Santa Cruz[b]
MFN2	Mouse Monoclonal	1:1000	sc-100560	Santa Cruz[b]
OPA1	Mouse Monoclonal	1:1000	sc-393296	Santa Cruz[b]
DRP1	Mouse Monoclonal	1:1000	sc-271583	Santa Cruz[b]
Parkin	Mouse Monoclonal	1:1000	sc-32282	Santa Cruz[b]
PINK1	Mouse Monoclonal	1:1000	sc-517353	Santa Cruz[b]
BNIP3	Mouse Monoclonal	1:1000	sc-56167	Santa Cruz[b]
Cytochrome C	Mouse Monoclonal	1:1000	sc-13156	Santa Cruz[b]
COX4I2	Mouse Monoclonal	1:1000	sc-100522	Santa Cruz[b]
SOD2	Mouse Monoclonal	1:1000	sc-133134	Santa Cruz[b]
MtTFA	Mouse Monoclonal	1:1000	sc-376672	Santa Cruz[b]
Caspase 1	Mouse Monoclonal	1:1000	sc-56036	Santa Cruz[b]
Caspase 3	Mouse Monoclonal	1:1000	sc-271028	Santa Cruz[b]
Bcl-2	Mouse Monoclonal	1:1000	sc-7328	Santa Cruz[b]
Bcl-XL	Mouse Monoclonal	1:1000	sc-8392	Santa Cruz[b]

[a]Cambridge, United Kingdom

[b]Dallas, Texas, USA

Table 2

Characteristics of secondary antibodies

Expression system	Conjugate	Species/Clone	Dilution	Catalog #	Supplier
Donkey/IgG	Alexa Fluor® 680	Rabbit Polyclonal	1:10,000	A10043	Invitrogen[c]
Rabbit/IgG	Alexa Fluor® 680	Mouse Polyclonal	1:10,000	A27031	Invitrogen[c]
Donkey/IgG	IRDye® 800CW	Rabbit Polyclonal	1:10,000	926-32213	LI-COR[d]

[c]Thermofisher Scientific, USA

[d]Nebraska, USA

Table 3

Stock and working concentrations of treatments

Treatments	Stock concentration	Working concentration (in 1% FBS-containing medium)
ODE	100% in HBSS	1%
EP	5 mM in ringer's solution	2.5 μM
MA	1 mM in DMSO	10 μM